

Uncovering the Active Species in Amine-Mediated CO₂ Reduction to CO on Ag

Graham Leverick, Elizabeth M. Bernhardt, Aisyah Ilyani Ismail, Jun Hui Law, A. Arifutzzaman, Mohamed Kheireddine Aroua, and Betar M. Gallant*



Cite This: ACS Catal. 2023, 13, 12322–12337



Read Online

ACCESS |

Metrics & More

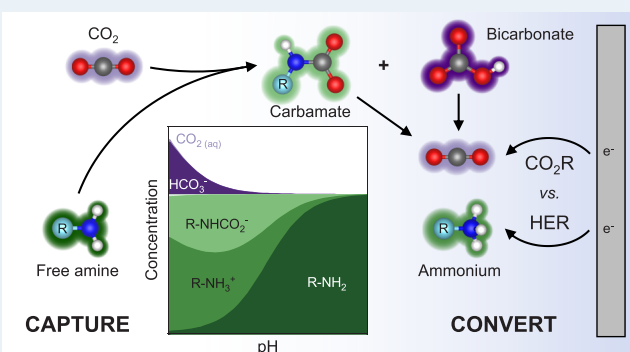
Article Recommendations

Supporting Information

ABSTRACT: Electrochemical reactive capture of CO₂, which integrates CO₂ capture with its conversion directly from amine and other capture solutions, is of growing interest to enable net zero and eventually negative greenhouse gas emissions. While integration has been proposed to mitigate certain energy penalties and inefficiencies that accrue when capture and conversion are decoupled, integration introduces considerable complexity to the electrochemical process due to the number of possible reactant participants, especially in an aqueous-based capture solution. Moreover, the influence of amine-based sorbents on CO₂ reduction (CO₂R) mechanisms is not well-understood, making rational design elusive at present. In this work, we reveal the governing parameters and active species in amine-mediated CO₂ conversion

as an essential initial step toward improving these processes. We first demonstrate the critical influence of CO₂ partial pressure of the capture stream on the resulting solution pH, which directly affects amine speciation and the Faradaic efficiency of CO production on Ag. Moreover, by considering amines of different pK_a and with different propensities to form the amine-CO₂ adduct carbamate, we show that dissolved CO₂ is the active species for CO₂R in amine-containing solutions, enabling some capture solutions to have comparable CO₂R selectivity and kinetics to amine-free bicarbonate solutions. As a result, amines can serve as a reservoir of dissolved inorganic carbon that can replenish dissolved CO₂ as it is consumed during CO₂R, alleviating mass transfer/transport limitations without directly participating electrochemically.

KEYWORDS: CO₂ capture, CO₂ conversion, electrochemical reduction, reactive capture, amine sorbents



INTRODUCTION

Technologies that can capture CO₂ from flue gas or directly from the atmosphere, while enabling conversion into inert minerals for sequestration or upgraded liquid or gas products, are vital for transitioning toward net zero and eventually negative greenhouse gas emissions. In particular, electrochemical reduction of CO₂ (CO₂R) into fuels or chemical feedstocks like carbon monoxide (CO), methanol, ethanol, or ethylene could be cost-competitive with the current market rates of these chemicals.¹ When coupled with renewable energy like wind, such products could be carbon neutral or even carbon negative.² Conventional approaches to CO₂R utilize decoupled capture and conversion processes in which dilute CO₂ is first captured by a liquid sorbent, then regenerated via a thermal-swing process to yield back pure CO₂ and pressurized, prior to serving as the feedstock for electrochemical CO₂R in a separate downstream process. Unfortunately, even relatively mature technologies for CO₂ capture, e.g., those using monoethanolamine (MEA)-based scrubbing solutions, are energetically and capitally intensive,³ requiring large amounts of energy (88–200+ kJ/mol of CO₂)^{4,5}

in the form of thermal energy from steam⁶) to regenerate the amine solution and release the captured CO₂. Emerging technologies that aim to integrate these capture and electrochemical conversion processes (a subcategory of “reactive capture”^{7,8}) can, in theory, achieve process intensification by replacing thermal regeneration with an immediate electrochemical process conducted on CO₂ in the captured state. Such integration has the additional merit of enabling energy requirements across both the capture and conversion processes to be solely sourced from renewables like wind and solar, making these processes fully electrified and also independent of a steam supply.^{9,10}

While promising, such integrated approaches introduce considerable complexity for reaction design because a wide

Received: June 1, 2023

Revised: August 16, 2023

Published: September 6, 2023



range of potential electrochemically active species can be present in the capture solution when loaded with CO₂. These include the solvent (e.g., H₂O); various amine species such as free amine (R—NH₂), carbamate (R—NHCO₂[−]), carbamic acid (R—NHCO₂H), and ammonium cations (R—NH₃⁺); as well as inorganic CO₂-derived species like carbonate (CO₃^{2−}), bicarbonate (HCO₃[−]), and dissolved CO₂ gas.¹⁰ Moreover, as the study of reactive capture systems is still in its infancy, many important fundamental questions remain. These include essential matters of how the capture environment impacts the resulting electrochemistry, including but not limited to the possible role of the amine itself. To address these vital open questions, we herein study the influence of accessible solution-state handles—CO₂ partial pressure, pH, the properties of the amine, and the resulting solution speciation—on CO₂R to CO on Ag catalysts. While other products may in theory be possible, prior efforts have focused mainly on CO₂-to-CO formation in amine capture solutions,^{11–13} making this reaction of highest relevance at present. Additionally, the simple 2e[−] reduction of CO₂ to CO on weakly binding catalysts like Ag and Au^{14,15} is well-understood in aqueous, amine-free CO₂R, enabling us to better isolate the influence of the amine on the reaction.

In amine-free electrolytes, CO₂R reduction to CO on Au and Ag electrodes¹⁶ is limited by the chemical or electrochemical adsorption of dissolved CO_{2,aq}. On Au electrodes, both Ringe et al.¹⁷ and Verma et al.¹⁸ have shown that the CO partial current density is invariant with pH on an SHE scale, consistent with the rate-determining step (RDS) being pH-independent. Wuttig et al.¹⁹ have shown that the CO partial current density exhibits a first-order dependence on the CO₂ partial pressure but a zeroth-order dependence on HCO₃[−] concentration, whereas Dunwell et al.²⁰ have used ¹³C isotopic labeling to show that the evolved CO on Au was isotopically similar to dissolved CO_{2,aq} but not HCO₃[−] or the CO₂ gas in the cell headspace (over the timescale of their experiments). Taken together, these findings support the interpretation that the RDS for CO₂R to CO in amine-free electrolytes involves dissolved CO_{2,aq}. Ringe et al.¹⁷ additionally used multi-scale modeling to argue that this RDS was the chemical adsorption of CO_{2,aq} via CO₂ + * → CO₂*, while others^{18,19} have proposed that the RDS is the coupled adsorption-electron transfer via CO₂ + e[−] + * → CO₂−*. Regardless of the exact mechanism, the kinetics of CO₂R to CO on Au electrodes in amine-free electrolytes is limited by the adsorption of dissolved CO_{2,aq}. Given that Au and Ag electrodes show similar reaction pathways¹⁵ and Faradaic efficiency (FE) for CO production¹⁶ during CO₂R stemming from their similar binding affinity,^{14,15} CO₂R to CO on Ag electrodes is similarly limited by the adsorption of dissolved CO_{2,aq}.

In contrast, there is yet to be consensus on the active species for CO₂R-to-CO in amine-containing aqueous electrolytes. A key question involves whether the CO₂-loaded amine, i.e., carbamate which forms from the enthalpically favorable reaction (~−80 to −100 kJ/mol²¹) between the free amine and CO₂, bears CO₂ to the electrode surface and therefore functions as an active species. On the one hand, Chen et al.,²² Kim et al.,¹² and Shen et al.²³ proposed that the CO₂R reaction occurred via electron transfer to dissolved CO_{2,aq} in aqueous MEA-containing electrolytes. Alternatively, Lee et al.¹¹ proposed that aqueous amine-coordinated-CO₂ (carbamate) was responsible for the formation of CO as the electrolytes in their study were sparged with N₂ to reduce the concentration

of dissolved CO₂ in the bulk electrolyte. It is also unclear if and how the amine's chemical structure can alter CO₂R. Kim et al.¹² showed that aqueous solutions with different amines yielded different CO FEs, which were ascribed to ammonium cations of decreasing effective radius leading to stronger stabilization of the CO₂[−] intermediate on the electrode surface. Enhanced CO₂R kinetics with cations of smaller effective radius has also been observed with alkali metal cations in amine-free electrolytes,^{24,25} as well as when adding alkali metal chloride salt to MEA-containing solutions.¹¹ Abdinejad et al.¹³ also proposed that some amines, like ethylenediamine (EDA), could catalytically promote CO₂R to CO on Cu.

In nonaqueous amine solutions, prior work from a subset of the authors^{26,27} showed increased cathodic current densities in cyclic voltammograms in Li-, Na-, and K-containing dimethyl sulfoxide electrolytes when both 2-ethoxyethylamine (EEA) and CO₂ were present (i.e., when carbamate was present), in contrast to EEA only (without CO₂) or with CO₂ only (without EEA). Such increased current density suggested that carbamate could be active for CO₂R to Li₂CO₃ + C on carbon electrodes in nonaqueous media; however, dissolved CO₂ was also suggested to play an important role that was not understood at the time of that work. Bhattacharya et al.²⁸ also observed enhanced cathodic current density in the presence of carbamate or carbamic acid in tetrabutylammonium-based acetonitrile electrolytes on carbon electrodes. On the other hand, Pérez-Gallent et al.²⁹ observed that removal of dissolved CO₂ from aminomethyl propanol (AMP)-containing propylene carbonate electrolytes by N₂ sparging yielded cathodic current densities on Pb electrodes that were similar to the background electrolyte, leading to the argument that dissolved CO₂ was responsible for CO₂R to formate, glycolate, and oxalate in their study. We note that the sterically hindered AMP does not readily form carbamate,³⁰ which may rationalize this difference. Nevertheless, the influence of amines on CO₂R remains an open question, which may depend significantly on the electrolyte (aqueous vs nonaqueous) as well as the electrode surface. Another important discrepancy between studies relates to the CO₂ saturation conditions of the electrolyte, where some studies saturate under pure CO₂,^{12,22} while others seek to remove dissolved CO₂ through subsequent sparging with N₂.^{11,29}

In this work, we leverage systematic studies on Ag catalysts to elucidate the differences between CO₂R in reactive capture solutions and conventional, amine-free CO₂R. We first demonstrate the critical role of the CO₂ partial pressure of the capture stream on the resulting CO₂-loaded solution pH. Using ¹H and ¹³C NMR, as well as a vapor–liquid equilibrium (VLE) model, we quantify in detail the pH-dependent speciation, showing that capture solutions derived from atmospheric CO₂ partial pressures contain mostly carbamate, whereas laboratory-prepared capture solutions saturated under pure CO₂ contain substantially heightened proportions of bicarbonate. Through electrochemical studies, we find that the pH dramatically influences the FE of CO production. Significantly, the CO FE at pH values associated with atmospheric CO₂ partial pressure is negligible (<0.1%) but can increase greatly in solutions saturated with pure CO₂. Moreover, by considering amines of different pK_a and with different propensities to form carbamate, we show that the examined amine-containing solutions can reach but not significantly exceed the CO₂R selectivity and kinetics of amine-free bicarbonate solutions, which stems from the fact

that CO₂, not carbamate, is the active species. Through this work, we provide clarity on the influence of amines during CO₂R from reactive capture solutions, as well as provide guidance and best practices for this exciting, developing field.

EXPERIMENTAL PROCEDURES

Chemicals. Potassium chloride (Sigma-Aldrich, anhydrous, Redi-Dri, ACS reagent, ≥99%), potassium bicarbonate (Sigma-Aldrich, ACS reagent, 99.7%), potassium carbonate (Thermo Scientific, ACS reagent, anhydrous, >99%), MEA (Sigma-Aldrich, ACS reagent, ≥99.0%), monoethanol amine hydrochloride (“MEAHC”), Sigma-Aldrich, anhydrous, Redi-Dri, ≥99.0%), β-aminopropionitrile (“BAPN”, TCI America, stabilized with K₂CO₃ ≥ 98.0%), n-butylamine (“n-BA”, Sigma-Aldrich, 99.5%), n-butylamine hydrochloride (“n-BAHCl”, TCI America, ≥98.0%), (+/-)-2-amino-1-propanol (“2A1P”, Thermo Scientific, >98%), 2-amino-2-methyl-1-propanol (“AMP”, Thermo Scientific, >99%), N,N-dimethylethanamine (“DMAE”, Sigma-Aldrich, ≥99.5%), hydrochloric acid (Fisher Chemical, ACS Plus, 37% w/w), potassium hydroxide (Sigma-Aldrich, reagent grade, 90%), potassium phosphate monobasic (H₂KPO₄, Thermo Scientific, ACS reagent, ≥99.0%), and potassium phosphate tribasic (K₃PO₄, Thermo Scientific, anhydrous, ≥97.0%) were used as received. N₂ gas (Airgas, “Ultra High Purity”, <1 ppm O₂, CO, CO₂) and CO₂ (Airgas, “Research Grade”, <1 ppm O₂, CO) were used as received.

Electrochemical Measurements. Electrochemical cells were constructed with a custom-made, jacketed H-cell, where the catholyte and anolyte were separated by a 24 mm diameter piece of Nafion 117 (FuelCellStore, please see discussion of membrane influence in the *Supporting Information*). The anolyte compartment contained 30 mL of 1 M KOH and a Pt counter electrode. The catholyte compartment contained 30 mL of electrolyte, a PTFE stir bar, an Ag foil working electrode (as described in the *Supporting Information*), a fritted Ag/AgCl reference electrode (Pine Research, with a potential of +0.199 V_{SHE}), and a pH electrode (YSI, Science pH-Micro). The pH and electrolyte temperature were monitored during the experiment with a YSI TruLab pH 1310 that had been calibrated with pH 4.0, 7.0, and 10.0 reference solutions (Micro Essential). The headspace of the cell was sealed with a custom gasket (New England Die Cutting), and gas was sparged with a custom-built apparatus composed of stainless steel 316 Swagelok fittings, stainless steel 316 tubing, and polyether ether ketone (PEEK) tubing, where only the PEEK tubing was in contact with the electrolyte.

Following assembly of the cell, the volume of the gas headspace was determined using pressure swing experiments (see *Supporting Information* for details), and then the cell was sparged with N₂ at 200 sccm using a mass flow controller (Alicat Scientific) for at least 15 min to remove any O₂. Next, CO₂ gas was sparged until the targeted pH was reached, following which N₂ gas was flowed to remove excess CO₂ gas and the cell was sealed and allowed to equilibrate for at least 5 min. During this time, electrochemical impedance spectroscopy (EIS) was performed to determine the iR drop. Next, a potentiostatic measurement was performed (typically at -1.30 V_{SHE}) using 90% iR correction based on the measured iR drop where the total charge passed was fixed to 0.9 mAh. As shown in *Table S1*, using 90% iR correction resulted in true applied potentials that were within 26 mV of -1.30 V_{SHE}, with most within 5 mV. Following the potentiostatic measurement, gas

bubbles adhered to the working electrode were mechanically disrupted, and any bubbles trapped in the “H” part of the cell were reunited with the gas headspace by tipping the cell. The headspace was allowed to equilibrate for at least 5 min, following which a 5 mL gastight syringe (Restek) was used to extract a sample of the headspace and analyzed using an Agilent 7890B GC Gas Chromatograph (2× HP-PLOT Q PT and 1× HP-PLOT Molsieve columns with a methanizer to increase sensitivity to CO₂ and CO gases). A full description of the gas quantification procedure can be found in the *Supporting Information*. All electrochemical measurements were performed using a Biologic VSP potentiostat while stirring the catholyte with a PTFE stir bar at 200 rpm. For 60 °C measurements, heated water (Julabo BC4) was flowed through the catholyte jacket such that the temperature read by the temperature probe in the pH electrode (YSI, Science pH-Micro) gave a temperature of 60 ± 1 °C. The Ag/AgCl reference electrode was assumed to have a potential of -0.164 V_{SHE} at 60 °C based on a temperature coefficient of 1.01 mV/°C.

NMR Quantification of Speciation. All NMR spectra were collected with a three-channel Bruker Avance Neo spectrometer operating at 500.34 MHz. NMR samples were prepared by mixing 0.63 mL of the sample with 70 μL of a D₂O/TMSP-d4/Gad solution. The D₂O/TMSP-d4/Gad solution was prepared by mixing 1 mL of D₂O + 0.75 w% TMSP-d4 (Sigma-Aldrich, 99.9 atom % D, with 0.75 wt. % 3-(trimethylsilyl)propionic-2,2,3,3-d₄ acid, sodium salt), with an additional 15 mg of TMSP-d4 (Thermo Scientific, 2,2,3,3-d(4)-3-(trimethylsilyl)propionic acid sodium salt, 98+ atom % D) and 1.8 mg of (3 mM) Gadodiamide (“Gad”, Apexbio Technology, gadolinium-based contrast agent). Additional TMSP-d4 was added to aid referencing the chemical shift in ¹³C NMR, while Gadodiamide was added to shorten the T₁ relaxation time of ¹³C nuclei (*Figure S1*) allowing for semi-quantitative analysis with higher signal-to-noise ratios and shorter recycle delays. In order to achieve semi-quantitative ¹³C NMR, we used a single pulse program (zgig) with D₁ = 12 s, which was >5 times longer than the slowest T₁ relaxation observed when Gadodiamide was present, ~ 2.3 s (*Figure S1*). Spectra were collected with 64 scans to achieve signal-to-noise ratios >100 and an optimized pulse width P₁ = 12 μs. Semi-quantitative ¹³C NMR relies on no significant variation in the isotopic abundance of ¹²C/¹³C, which was previously confirmed by Kortunov et al.³¹ for MEA, DMAE, and CO₂ gas and is assumed in this work. The accuracy of our semi-quantitative ¹³C NMR measurements was assessed through comparisons between the carbamate concentration from both ¹H and ¹³C NMR, which showed excellent agreement with deviations <1% (*Figures S2–S4*), as well as from a charge balance analysis of the speciation (where [R-NH₃⁺] - [R-NHCO₂⁻] - [HCO₃⁻] - 2[CO₃²⁻] is expected to be <10 mM for pH values <12), which suggest quantitative errors <10% with most <5%. All chemical shifts were referenced based on the chemical shift of TMSP-d4 which we took as δ_{TMSP-d4}^{1H} ≡ 0 and δ_{TMSP-d4}^{13C} = -2.66 ppm (by comparison to TMS in *Figure S5*). Such non-zero δ_{TMSP-d4}^{13C} was unexpected but resulted in ¹³C chemical shifts that agreed well with those reported in the literature.^{31,32} The slight dilution of the sample as well as the presence of TMSP-d4 and Gad had negligible influence on the resulting species quantification (*Figures S2–S4*) nor did the

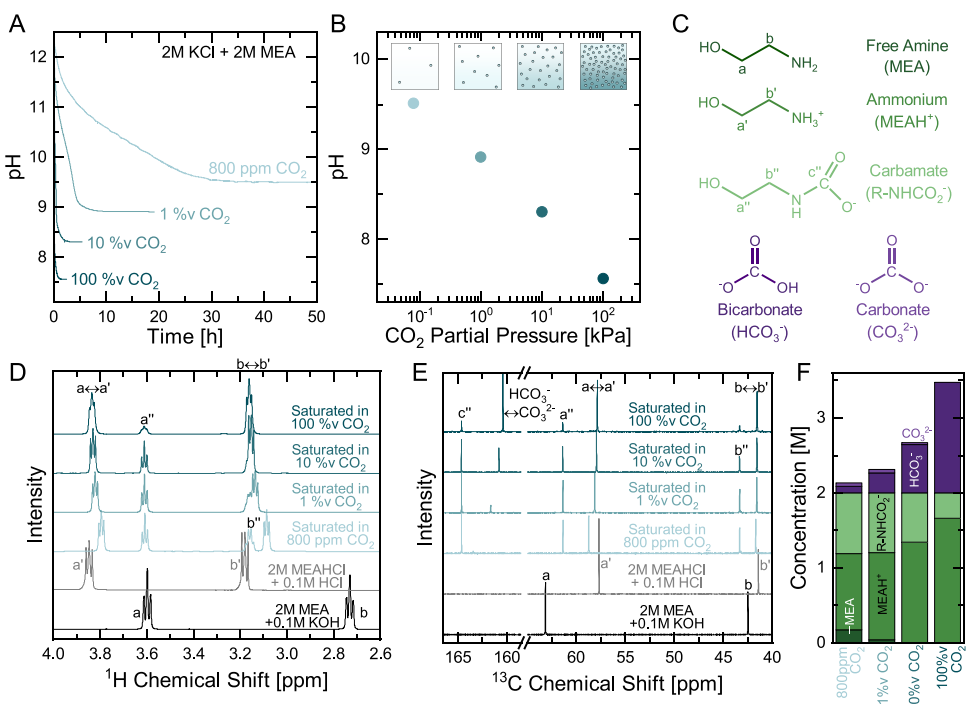


Figure 1. (A) pH of 2 M KCl + 2 M MEA solutions vs time. At the start of the experiment, all solutions are at pH \sim 12.3 following N₂ saturation for 15 min. At $t = 0$, a gas flow containing 800 ppm, 1 v% CO₂, 10%v CO₂, or 100%v CO₂ begins, and the pH is monitored until equilibrium is reached. (B) Equilibrium pH from (A) vs the CO₂ partial pressure in the headspace above the solution. The calculated CO₂ partial pressure assumes atmospheric pressure (101.325 kPa) and 100% relative humidity. (C) Summary of amine and (bi)carbonate species present in the solution and nomenclature used to identify NMR peaks in (D) and (E). All peak assignments are based on the work of Fan et al.³² and Kortunov et al.³¹ (D) ¹H NMR spectra of the 2 M KCl + 2 M MEA solutions after reaching equilibrium in (A). Reference spectra of 2 M MEA + 0.1 M KOH and 2 M MEA + 0.1 M HCl are included, where only free amine and ammonium cations are expected, respectively, based on the measured pH and stoichiometry. (E) ¹³C NMR spectra of the 2 M KCl + 2 M MEA solutions after reaching equilibrium in (a). (F) Quantification results based on the chemical shifts and integral areas from ¹H and ¹³C NMR spectra in (D) and (E). A full description of the procedure can be found in the Supporting Information.

composition of the gas in the headspace of the NMR tube (Figure S6). Full details on how the resulting ¹H and ¹³C NMR spectra were used to quantify the concentrations of [R-NH₂], [R-NH₃⁺], [R-NHCO₂⁻], [HCO₃⁻], and [CO₃²⁻] for each amine can be found in the Supporting Information.

VLE Model of Amine Speciation. A VLE model of the amine speciation was developed based on the chemical equilibria described in the main text, as well as charge and mass balance expressions. The balance of charge is given by

$$\begin{aligned} [\text{RNH}_3^+] + [\text{Cation}] + 10^{-\text{pH}} \\ = [\text{RNHCOO}^-] + [\text{HCO}_3^-] + 2[\text{CO}_3^{2-}] + [\text{Anion}] \\ + 10^{\text{pH}-\text{K}_w} \end{aligned}$$

The amine mass balance is given by

$$\begin{aligned} [\text{RNH}_2]_{\text{total}} = [\text{RNH}_2] + [\text{RNH}_3^+] + [\text{RNHCO}_2^-] \\ + [\text{RNHCO}_2\text{H}] \end{aligned}$$

where [RNH₂]_{total} is given by the amine concentration of the prepared solution. A full description of the model equations as well as all parameters used can be found in the Supporting Information.

RESULTS

CO₂ Partial Pressure Determines Equilibrium pH and Amine Speciation. The goal of reactive capture systems is to eliminate the thermal regeneration step and perform electro-

chemistry immediately after capturing CO₂ from sources such as flue gas (with 12–14 v% CO₂)¹⁰ or directly from the atmosphere (with \sim 400 ppm CO₂).³³ However, both the equilibrium pH and speciation of amine-based capture solutions vary significantly with CO₂ partial pressure in the capture stream. This relationship is illustrated in aqueous 2 M KCl + 2 M MEA solutions, where CO₂-free solutions had a pH of \sim 12.3. Bubbling 100 v% CO₂ into the solution led to a pH decrease over time, with equilibrium reached after \sim 2 h. The same process required \sim 40 h for dilute 800 ppm CO₂ (Figure 1A). Overall, the equilibrium pH was found to decrease significantly with increasing CO₂ partial pressure from a pH of 9.5 for 81 Pa CO₂ to 7.6 for 100 kPa (Figure 1B). These data illustrate that the properties of the reactive capture solution are highly sensitive to the gas-phase capture environment. In particular, capture solutions derived from direct air capture differ substantially from those from flue gas, as well as those saturated under pure CO₂ in a laboratory.

To further probe the influence of CO₂ partial pressure on the composition of MEA solutions, the solution-phase speciation was quantified through ¹H and ¹³C NMR experiments. ¹H NMR spectra of the same 2 M KCl + 2 M MEA solutions saturated in 800 ppm–100%v CO₂ (Figure S7) showed a large H₂O peak in the range of 4.8 to 4.9 ppm vs TMSP, a small broad peak at \sim 5.35 ppm attributable to the amine-hydrogen in carbamate (R-NH-CO₂⁻), as well as various multiplets in the range of 3–4 ppm, attributable to the ethyl-hydrogens (HO-CH₂-CH₂-R) of the free amine,

ammonium cation, and carbamate³² (Figure 1C,D). It is notable in Figure 1D that the chemical shift of the ethyl-hydrogens of free amine and ammonium species in these CO₂-loaded solutions ($b \leftrightarrow b'$, which are in fast exchange) is much more similar to that of a solution of 2 M MEA + 0.1 M HCl (used as reference for ammonium cations) than that of 2 M MEA + 0.1 M KOH (used as reference for free amine). This indicates that only a small amount of free amine is present in 2 M KCl + 2 M MEA at all considered CO₂ partial pressures and that the majority of the non-carbamate species exist as ammonium cations. Note that the reference solutions above contained either 0.1 M KOH or 0.1 M HCl, respectively, to ensure that the solution pH was well above (or below, respectively) the pK_a of MEA such that only one species of the MEAH⁺ \leftrightarrow MEA + H⁺ equilibrium was present. Distinct signals from the protons in the R-NH₂ and R-H₃⁺ moieties are absent as they are in fast exchange with water (Figure S8). Also of note in Figure 1D is that the peak height of carbamate (the triplet at \sim 3.6 ppm vs TMS reference denoted as a" in Figure 1D) decreases monotonically between 800 ppm, 1 v%, 10%v CO₂, and 100%v CO₂, indicating decreasing carbamate species with increasing CO₂ partial pressure.

¹³C NMR measurements revealed increasing proportions of (bi)carbonate species with increasing CO₂ partial pressure, where bicarbonate forms from the hydrolysis of carbamate given by the equilibrium R-NHCO₂⁻ + H₂O \leftrightarrow R-NH₂ + HCO₃⁻.³⁴ ¹³C NMR spectra of 2 M KCl + 2 M MEA solutions saturated in 800 ppm–100%v CO₂ (Figure 1E) showed four peaks in the range of 40–65 ppm attributable to the ethyl carbon (HO-CH₂-CH₂-R) of the free amine, ammonium cation, and carbamate. A peak was also present at 164.6 ppm, attributable to the CO₂ adduct of carbamate, as well as one in the range of 160 to 163.5 ppm attributable to the fast exchange of carbonate and bicarbonate species^{31,32} (Figure 1E). Quantifying the speciation based on the chemical shifts and integral areas from ¹H and ¹³C NMR spectra (full description in the Supporting Information) confirmed that the amount of carbamate decreases from 0.81 M for the 800 ppm CO₂-saturated solution to just 0.34 M for the 100 v% CO₂-saturated solution (Figure 1F). Conversely, the amount of bicarbonate increased significantly from only 0.08 to 1.5 M for these solutions, respectively. In the remainder of this work, pH is used as an independent variable, where a given solution pH can be understood to represent the state of a capture solution saturated under some corresponding equilibrium partial pressure of CO₂ (Figures 1B and S9).

VLE Model Rationalizes the Partial Pressure-Dependent pH and Speciation. We next investigated the temporal pH-dependent speciation of 2 M KCl + 2 M MEA solutions, beginning from CO₂-free solutions and gradually increasing the CO₂ loading by sparging over time at a fixed inlet CO₂ partial pressure (100 v%). ¹H and ¹³C NMR spectra were collected in the pH range of 12.3 (CO₂-free) to 7.6 (saturated under pure CO₂) and quantified as above. As shown in Figure 2A, as the pH decreased from 12.3, primarily \sim equimolar carbamate (R-NHCO₂⁻) and ammonium (MEAH⁺) formed, with just a small amount of bicarbonate (HCO₃⁻) and carbonate (CO₃²⁻). However, as the pH reached \sim 9, the carbamate concentration reached a maximum and began to decrease thereafter, whereas the concentration of ammonium continued to increase. Decreasing carbamate was accompanied by a sharp increase in the amount of bicarbonate species, which increased

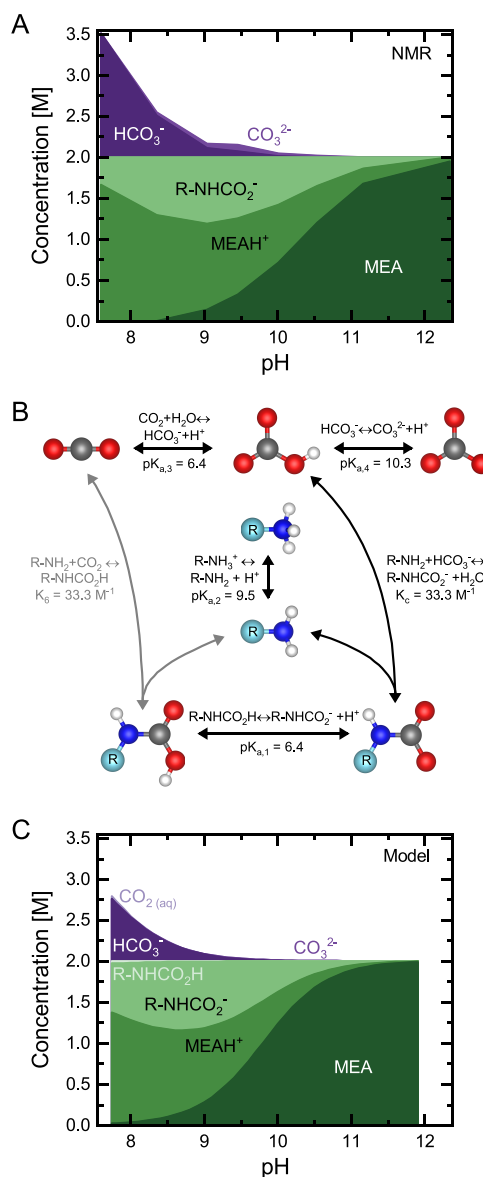


Figure 2. (A) Concentration of free amine (MEA), ammonium (MEAH⁺), carbamate (R-NHCO₂⁻), carbonate (CO₃²⁻), and bicarbonate (HCO₃⁻) vs pH of a 2 M KCl + 2 M MEA solution bubbled with pure CO₂. Quantifications from ¹H and ¹³C NMR spectra; the quantification methodology can be found in the Supporting Information. (B) Overview of reactions, equilibrium constants, and pK_a values used for the VLE model. Reactions in black are explicitly defined in the model, whereas those in gray are redundant and can be derived from the other reactions using the principle of microscopic reversibility (i.e., $K_6 = (10^{pK_{a,1}} - 10^{pK_{a,3}})K_c$). Parameter values are from Conway et al.³⁵ (pK_{a,1}), Gupta and Svendsen³⁶ (pK_{a,2}), England et al.³⁷ (pK_{a,3} and pK_{a,4}), and du Preez et al.³⁸ (K_c). (C) Modeled concentrations of MEA, MEAH⁺, R-NHCO₂⁻, R-NHCO₂H, CO₃²⁻, HCO₃⁻, and dissolved CO₂ from the VLE model. Model descriptions and parameters can be found in the Supporting Information.

monotonically until the solution became fully CO₂-saturated at a pH of 7.6.

To rationalize the pH-dependent speciation observed in Figure 2A, a VLE model was developed based on the known reactions among the species and published values of equilibrium constants and pK_a (Figure 2B). A full description of the model is provided in the Supporting Information;

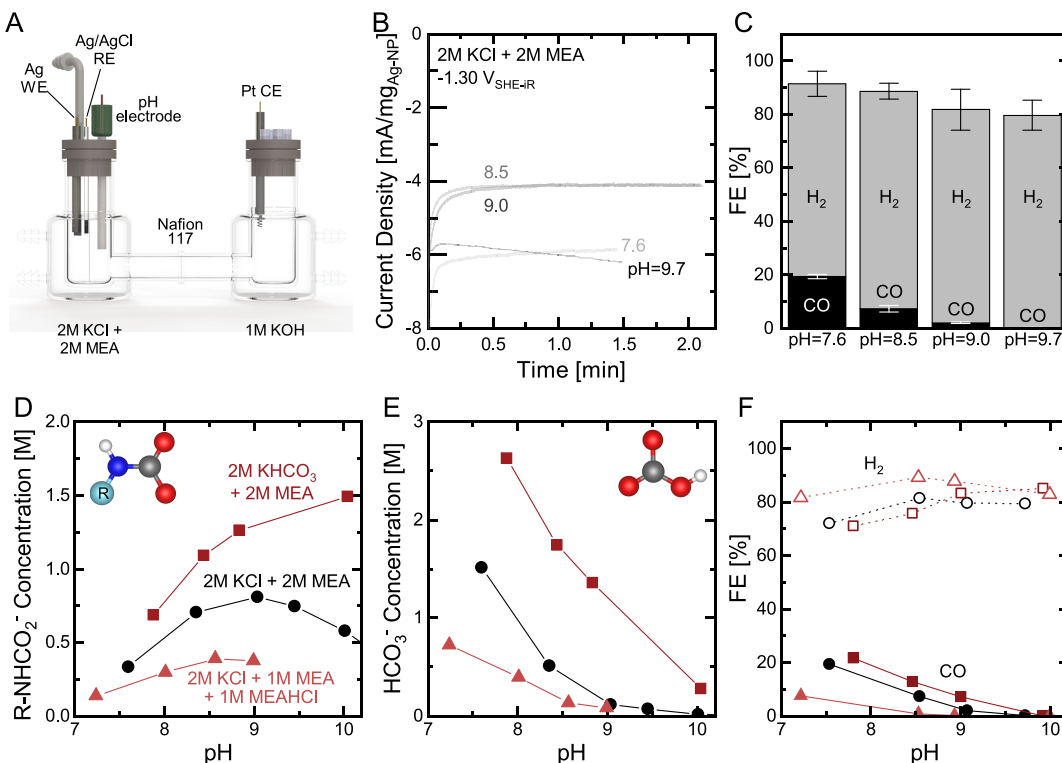


Figure 3. (A) Schematic of the experimental setup used for electrochemical measurements. The setup consisted of an H-cell with 2 M KCl + 2 M MEA catholyte and 1 M KOH anolyte separated by a Nafion 117 membrane with Ag nanoparticles on Ag foil as the working electrode (**Figure S10**), an Ag/AgCl reference electrode, a Pt counter electrode, and a pH electrode submerged in the catholyte. (B) Current density vs time from potentiostatic measurements at $-1.30\text{ V}_{\text{SHE-IR}}$ in 2 M KCl + 2 M MEA with pH ranging from 9.7 to 7.6. The current is normalized by the mass of deposited Ag nanoparticles and charge passed in each experiment is fixed at 0.9 mAh. (C) FE of CO and H₂ production from the potentiostatic measurements in (B). Product quantification was performed using GC. Error bars are the standard error of three independent measurements. (D) Concentration of carbamate (R-NHCO₂⁻), determined from NMR, vs pH for 2 M KCl + 2 M MEA (circle), 2 M KCl + 1 M MEA + 1 M MEAHCl (triangle), and 2 M KHCO₃ + 2 M MEA (square). (E) Concentration of bicarbonate from NMR vs pH. (F) FE of CO (filled symbols) and H₂ (open symbols) production vs pH from potentiostatic measurements at $-1.30\text{ V}_{\text{SHE-IR}}$. Details from NMR quantification, product quantification, and electrochemical experiments can be found in the **Supporting Information**.

briefly, the equilibria shown in **Figure 2B** were combined with charge and mass balance to generate a system of equations that could be uniquely solved as a function of pH. As shown in **Figure 2C**, the modeled speciation matches well with that determined by NMR (**Figure 2A**), although the model predicts somewhat less bicarbonate species but more carbamate. At pH values greater than the pK_a of MEAH⁺ ($\text{pK}_{\text{a},2} = 9.5^{36}$), the formation of ~equimolar carbamate and ammonium can be rationalized by the reaction between MEA and CO₂ to form carbamic acid (K₆), followed by the subsequent deprotonation of carbamic acid ($\text{pK}_{\text{a},1}$) by free amine, since $\text{pK}_{\text{a},1} < \text{pK}_{\text{a},2}$. The subsequent increase in bicarbonate at lower pH is best understood by combining the hydrolysis equilibrium K_c with the pK_{a,2} of MEAH⁺ to yield the acid-catalyzed carbamate hydrolysis equilibrium, given by $\text{R-NH}_3^+ + \text{HCO}_3^- \leftrightarrow \text{R-NHCO}_2^- + \text{H}_2\text{O} + \text{H}^+$. The “effective” equilibrium constant $K_{\text{c,eff}} = (10^{\text{pH}-\text{pK}_{\text{a},2}})K_c$ of this reaction increasingly favors carbamate hydrolysis as the pH decreases below pK_{a,2} (see **Supporting Information** for derivation). Notably, the acid-catalyzed hydrolysis of carbamate to bicarbonate enables the CO₂ loading to exceed 0.5 mol_{CO2}/mol_{MEA}, reaching 0.7 at pH 7.7 in the VLE model (**Figure 2C**). The proportion of carbamic acid predicted by the model is small at all pH values (**Figure 2C**), which agrees with no measurable changes in the chemical shift of carbamate species from ¹H and ¹³C NMR with pH. Finally, the modeled equilibrium CO₂ partial pressure

agrees with the findings presented in **Figure 1**, where atmospheric CO₂ partial pressures of ~400 ppm (40 Pa) correspond to a solution pH of 9.6, but this pH decreases to ~7.7 for pure CO₂ at atmospheric pressure (**Figure S9**). Next, we consider the influence of the capture solution pH (and corresponding changes in speciation) on the selectivity for CO and H₂ production during electrochemical reduction.

Higher FE for CO Formation Occurs at Lower pH. The FE of CO formation exhibited a strong inverse relationship with pH. Electrochemical experiments were conducted using an H-cell with 2 M KCl + 2 M MEA catholyte and 1 M KOH anolyte separated by a Nafion 117 membrane (**Figure 3A**). The working electrode consisted of a Ag nanoparticle/Nafion slurry deposited onto Ag foil (**Figures S10 and S11**), intentionally chosen to avoid possibly confounding effects of carbon. The Nafion binder used in the slurry led to increased CO FE relative to PTFE, as discussed further in the **Supporting Information**. Typical measurements consisted of a potentiostatic hold at $-1.30\text{ V}_{\text{SHE-IR}}$ until 0.9 mAh of charge had passed. For pH values between 9.7 and 7.6, as shown in **Figure 3B**, the current density was in the range of -4 to $-6\text{ mA}/\text{mg}_{\text{Ag-NP}}$, which corresponds to ~ 20 to $\sim 30\text{ mA/cm}^2_{\text{geo}}$. Gas chromatography (GC) was then used to quantify the FE of evolved H₂ and CO, as well as the CO₂ found in the headspace of the cell (quantification details are given in the **Supporting Information**). Significantly, the FE of CO formation at a pH of

9.7 was <0.1%. This low CO FE is remarkable as pH 9.7 is very similar to that expected from direct air capture (~9.6 in Figure S9), suggesting that capture-conversion directly from the atmosphere may be challenging. This number increased significantly to ~19% when the pH decreased to 7.6 (i.e., fully saturated with pure CO₂), indicating that the solution pH, as dictated by the CO₂ partial pressure of the capture stream, plays a critical role in determining product selectivity during CO₂R. Deviations of the total FE from 100% are attributed to evolved gases that are dissolved in the electrolyte, which can lead to errors >5% (see Supporting Information for details). When the potential was fixed at -0.70 V_{RHE-iR} instead of -1.30 V_{SHE-iR}, qualitatively similar trends for CO FE were observed, increasing from <0.2% at pH 10.0 to 28% at pH 7.6 (Figures S12 and S13). Additional discussion on the influence of using an SHE vs RHE scale is presented in the Supporting Information.

The relationship between the CO FE and the measured/modeled (Figure 2A,C) solution speciation was next inspected. Interestingly, the monotonic increase of CO FE as the pH drops from 9.7 to 7.6 (Figure 3C) is counter to the decreasing concentration of carbamate species over the same pH range (Figures 2A and 3D) but correlates well with increasing bicarbonate (Figures 2A and 3E). Similarly, the CO₂ partial pressure increased monotonically with decreasing pH from ~60 Pa at pH 9.7 to ~100 kPa at pH 7.6 (Figure S14). These CO₂ partial pressures were calculated based on the concentration of CO₂ detected in the headspace of the cell following electrochemistry assuming equilibrium, with the exception of the fully CO₂-saturated case (pH 7.6) which assumed atmospheric pressure and 100% relative humidity.

To further examine the relationship between speciation and CO FE, the electrolyte was modified by replacing the total 2 M MEA by 1 M MEA + 1 M MEAHCl (protonated amine). Having less free amine present in the solution resulted in the CO₂-free solution pH dropping from 12.3 (2 M KCl + 2 M MEA) to 10.0 (2 M KCl + 1 M MEA + 1 M MEAHCl). The speciation from NMR and the VLE model (Figure S15) indicated qualitatively similar pH-dependent trends as the baseline (2 M KCl + 2 M MEA) electrolyte, reaching maximum carbamate concentration at pH ~8.5, following which the bicarbonate concentration increased due to the hydrolysis of carbamate. However, the 1 M MEAHCl-substituted electrolyte showed lower concentrations of both carbamate and (bi)carbonate species (Figure 3D,E), consistent with less free amine to capture CO₂ to form carbamate and subsequently hydrolyze to form (bi)carbonate. As before, the 1 M MEAHCl-substituted electrolyte showed increasing CO FE with decreasing pH, e.g., from <0.1% at pH 10.0 to ~8% under CO₂ saturation at pH 7.2.

We also modified the 2 M KCl + 2 M MEA (baseline) electrolyte by replacing 2 M KCl with 2 M KHCO₃. This decreased the as-prepared solution pH to 10.4 but yielded qualitatively similar pH-dependent behavior except with higher overall concentrations of both carbamate (~1.5 M) and (bi)carbonate (~2.8 M) species from NMR and the VLE model (Figures 3D,E and S15). The elevated concentration of carbamate relative to the baseline solution is attributed to the hydrolysis equilibrium reaction given by R-NH₂ + HCO₃⁻ \leftrightarrow R-NHCO₂⁻ + H₂O (K_c in Figure 2B), where the addition of free amine and excess bicarbonate can lead to the formation of carbamate. Again, the CO FE increased with decreasing pH, from <0.1% at pH 10.0 to ~22% under CO₂ saturation at pH

7.8. In general (Figures 3F, S16, and S17), the CO FE increased with the trend MEAHCl-substituted < KCl/MEA (baseline) < KHCO₃-substituted, which is the same as the trend of both bicarbonate and carbamate concentration in each solution at fixed pH. Yet, it is particularly notable that in the solution with the highest carbamate concentration (KHCO₃/MEA at pH 10.0), there was negligible CO production, with FE <0.1%. Additionally, as pH decreased in all cases, the CO FE increased commensurate with bicarbonate concentration increasing, despite decreasing carbamate concentrations. Hence broadly, across all considered capture solutions, we observe a profound influence of the pH/equilibrium CO₂ partial pressure on the solution speciation and CO FE, where increased CO FE is correlated with decreased pH, increased bicarbonate concentration, and increased CO₂ partial pressure.

Amines of Varying pK_a and Propensity To Form Carbamate Have Similar CO Production to MEA. Other carbamate-forming primary amines of different pK_a were next examined to investigate the influence of amine properties on the resulting capture solution speciation and CO FE. In addition to MEA, we considered β -aminopropionitrile (BAPN) and *n*-butylamine (*n*-BA), which are structurally similar to MEA but have either lower or higher pK_a, respectively (Figure 4A). As expected, the pH of CO₂-free 2 M KCl + 2 M amine solutions increased from BAPN (11.2) to MEA (12.3) and *n*-BA (12.7), consistent with the increasing amine basicity. Through ¹H and ¹³C NMR measurements, the pH-dependent speciation of 2 M KCl + 2 M BAPN and 2 M KCl + 2 M *n*-BA (Figures 4B–E and S18) was again determined (peak assignment and quantification details in the Supporting Information). Comparing BAPN, MEA, and *n*-BA, solutions prepared with all three amines show qualitatively similar speciation trends with pH, but amines of increasing pK_a were shifted to higher pH values and showed a greater extent of carbamate hydrolysis to form bicarbonate. For instance, the concentration of bicarbonate when fully saturated with CO₂ increased with increasing amine pK_a from 0.33 M (BAPN) to 1.5 M (MEA) and 1.9 M (*n*-BA, Figures 4E and S18). A more detailed discussion of the influence of amine pK_a on speciation is presented in the Supporting Information. Similar to MEA, the CO FE monotonically increased with decreasing pH for both BAPN and *n*-BA (Figures 4F, S19, and S20). For instance, in 2 M KCl + 2 M BAPN, the CO FE increased from <0.1% at pH 8.7 to ~10% at pH 7.0, and in 2 M KCl + 2 M *n*-BA, the CO FE increased from 0.1% at pH 10.5 to ~19% at pH 7.8.

To further probe the influence of amine properties on the solution speciation and resulting CO FE, we next considered amines forming overall reduced concentrations of carbamate, such as primary amines with structures that sterically hinder the formation of carbamate or tertiary amines that are unable to form carbamate at all. Additional 2 M KCl + 2 M amine solutions were prepared with 2-amino-1-propanol (2A1P), aminomethyl propanol (AMP), and dimethylethanolamine (DMAE) (Figure 5A). These amines have similar pK_a to MEA (9.4,³⁶ 9.7,³⁶ and 9.2,³⁹ respectively, compared to 9.5 for MEA³⁶) but form less carbamate. As before, the pH of the CO₂-free solution increased with amine pK_a from 12.2 (DMAE) to 12.3 (2A1P and MEA) and 12.4 (AMP). Species quantification through ¹H and ¹³C NMR measurements indicated that primary amines with increasing steric hindrance yielded decreasing maximum concentrations of carbamate—from 0.81 M for MEA to 0.60 M for 2A1P and finally <40 mM

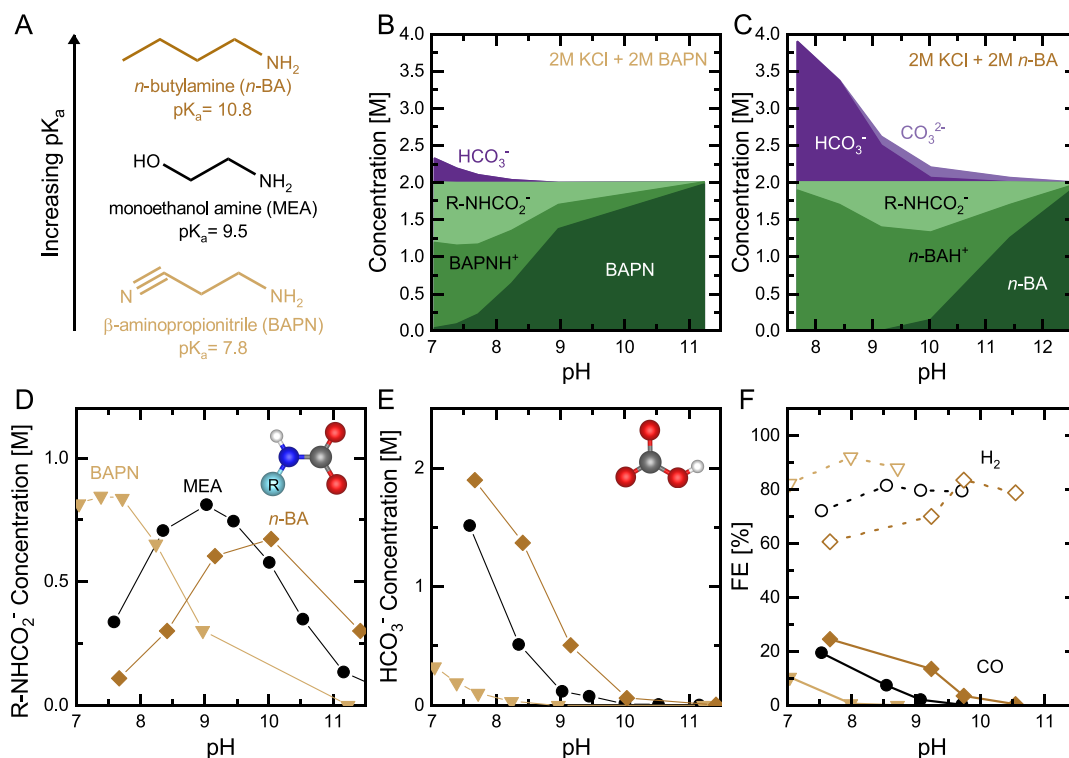


Figure 4. (A) Chemical structures of amines of increasing pK_a : BAPN ($pK_a = 7.8^{40}$), MEA ($pK_a = 9.5^{36}$), and *n*-BA ($pK_a = 10.8^{40}$). (B) Concentration of free amine (BAPN), ammonium (BAPNH⁺), carbamate (R-NHCO₂⁻), carbonate (CO₃²⁻), and bicarbonate (HCO₃⁻) vs pH of a 2 M KCl + 2 M BAPN solution bubbled with CO₂. (C) Concentration of *n*-BA, *n*-BAH⁺, R-NHCO₂⁻, CO₃²⁻, and HCO₃⁻ vs pH of a 2 M KCl + 2 M *n*-BA solution bubbled with CO₂. (D) Concentration of carbamate from NMR vs pH for 2 M KCl + 2 M amine with MEA (circle), BAPN (inverted triangle), and *n*-BA (diamond). (E) Concentration of bicarbonate from NMR vs pH. (F) FE of CO (filled symbols) and H₂ (open symbols) production vs pH from potentiostatic measurements at $-1.30\text{ V}_{\text{SHE}-\text{iR}}$. Details from NMR quantification, product quantification, and electrochemical experiments can be found in the Supporting Information.

for AMP (Figures 5B–D and S21). As expected, no carbamate species were observed in 2 M KCl + 2 M DMAE as DMAE is a tertiary amine that cannot form carbamate (Figure S21). The decreasing carbamate with increasing steric hindrance can be rationalized by decreasing values of the hydrolysis equilibrium constant K_c from 33.3 for MEA to 8.5 for 2A1P (Figure S22) and ~ 0.1 for AMP (Figure S23), where smaller values of K_c lead to increased hydrolysis of carbamate to bicarbonate. On the other hand, increasing steric hindrance of primary amines correlated with larger concentrations of (bi)carbonate species (Figure 5E); these (bi)carbonate species formed at higher pH values than with MEA (see additional discussion in the Supporting Information). Strikingly, the CO FE trend with pH was very similar for MEA, 2A1P, and AMP, increasing from $<0.3\%$ CO at pH ~ 10.0 for all three amines, to 19% for CO₂-saturated 2A1P, 18% for CO₂-saturated AMP, and 19% for CO₂-saturated MEA (Figures 5F, S24, and S25).

Across amines of varying pK_a and with differing propensities to form carbamate, the CO FE consistently increased with (1) decreasing pH (Figures 4F and 5F), (2) increasing bicarbonate concentration (Figures 4E and 5E), and (3) increasing CO₂ partial pressure (Figures S26 and S27). On the other hand, for all amines except BAPN, the CO FE (Figures 4F and 5F) trended in the opposite direction as the concentration of carbamate (Figures 4D and 5D). For BAPN, the concentrations of carbamate and bicarbonate (Figures 4D and 4E) as well as the CO₂ partial pressure (Figure S26) all increased with decreasing pH, making conclusions regarding correlations more challenging. Most notably, the CO FE for MEA, 2A1P,

and AMP showed almost identical trends with pH (Figure 5F), despite having very different carbamate concentrations (maximum 0.81 M for MEA vs <40 mM for AMP). This observation, combined with those previously, leads us to propose that carbamate does not directly participate in CO₂R in aqueous amine solutions on Ag.

Interestingly, while CO FE for DMAE also increased with decreasing pH, it reached a maximum of only 3.5% CO in the CO₂-saturated case (Figure 5F). Yet, the total current density at $-1.30\text{ V}_{\text{SHE}-\text{iR}}$ for DMAE-containing solutions (Figure S28) was much higher than that observed with 2A1P (Figure S24), AMP (Figure S25), or MEA (Figure 3B), suggesting that HER activity can vary substantially in the presence of different amines. To examine this more closely, the H₂ and CO partial current densities ($j_{\text{H}2}$ and j_{CO} , respectively) are next compared.

Ammonium Cations Can Enhance HER. Plotting the absolute value of the H₂ partial current density $|j_{\text{H}2}|$ vs pH for all 2 M KCl + 2 M amine solutions revealed that $|j_{\text{H}2}|$ shows significant amine-dependence (Figure 6A). For instance, $|j_{\text{H}2}|$ for MEA remains relatively constant with pH in the range of 3.5–5 mA/mg_{Ag-NP}, whereas $|j_{\text{H}2}|$ for DMAE is an order of magnitude higher, increasing from ~ 27 mA/mg_{Ag-NP} at pH 10.0 to ~ 60 mA/mg_{Ag-NP} at pH 7.8. This uniquely elevated $|j_{\text{H}2}|$ thus underlies the low CO FE with DMAE. We hypothesize that the observed amine-dependence of $|j_{\text{H}2}|$ is caused by ammonium cations serving as proton donors for HER, where ammonium cations (R-NH₃⁺) from different amines could have different HER activities. This hypothesis is consistent with the observed pH-dependence of $|j_{\text{H}2}|$ for

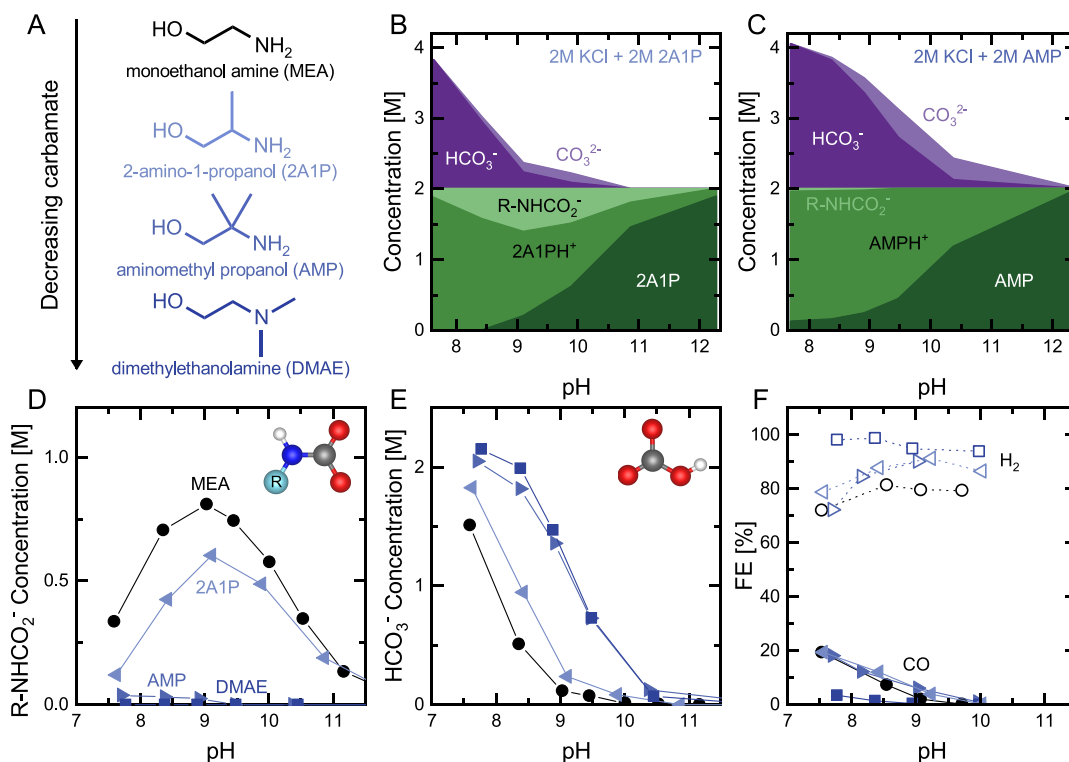


Figure 5. (A) Chemical structures of amines of decreasing propensity to form carbamate and MEA ($pK_a = 9.5^{36}$), 2A1P ($pK_a = 9.4^{36}$), AMP ($pK_a = 9.7^{36}$), and DMAE ($pK_a = 9.2^{39}$). (B) Concentration of free amine (2A1P), ammonium (2A1PH⁺), carbamate (R-NHCO₂⁻), carbonate (CO₃²⁻), and bicarbonate (HCO₃⁻) vs pH of a 2 M KCl + 2 M 2A1P solution bubbled with CO₂. (C) Concentration of AMP, AMPH⁺, R-NHCO₂⁻, CO₃²⁻, and HCO₃⁻ vs pH of a 2 M KCl + 2 M AMP solution bubbled with CO₂. (D) Concentration of carbamate from NMR vs pH for 2 M KCl + 2 M amine with DMAE (square), AMP (right-pointing triangle), 2A1P (left-pointing triangle), and MEA (circle). (E) Concentration of bicarbonate from NMR vs pH. (F) FE of CO (filled symbols) and H₂ (open symbols) production vs pH from potentiostatic measurements at $-1.30\text{ V}_{\text{SHE-IR}}$. Details from NMR quantification, product quantification, and electrochemical experiments can be found in the Supporting Information.

DMAE, where the increase in $|j_{\text{H}_2}|$ with decreasing pH is well-explained by the associated increase in ammonium cations with decreasing pH, leading to a very strong ($R^2 > 0.999$) correlation between $|j_{\text{H}_2}|$ and the concentration of ammonium cations (Figure S29). However, we note that these ammonium cations could also coordinate OH⁻ ions or H₂O, altering the kinetics of the Volmer step ($\text{H}_2\text{O} + \text{e}^- + * = \text{H}^* + \text{OH}^-$), which is anticipated to be rate limiting for HER on Ag from analogy to Au electrodes.⁴¹ Moreover, interpreting the pH-dependence of $|j_{\text{H}_2}|$ in Figure 6A is complicated by the fact that the overpotential for HER changes with pH since the applied potential was $-1.30\text{ V}_{\text{SHE-IR}}$ (Figure S13).

We next consider HER activity in the absence of ammonium cations to better understand HER kinetics in the presence of other possible proton donors—specifically H₂O and HCO₃⁻. We first tested two amine-free electrolyte compositions to determine the HER activity when H₂O is the primary proton donor (2 M KCl) and when HCO₃⁻ is also present as a potential proton donor (2 M KHCO₃). The pH of CO₂-free 2 M KCl (with 1 mM phosphate buffer to help stabilize the pH) was 6.7 and decreased to 5.2 upon saturation with CO₂. Significantly, $|j_{\text{H}_2}|$ for 2 M KCl was much lower than other electrolytes, remaining below 1.6 mA/mg_{Ag-NP} for all considered levels of CO₂ saturation (and pH), as shown in Figures 6A and S30. The low observed $|j_{\text{H}_2}|$ for 2 M KCl suggests that H₂O is a poor proton donor for HER at pH values between 5.0 and 7.0 on Ag electrodes. Meanwhile, the pH of amine-free 2 M KHCO₃ was ~ 9.1 after sparging with N₂ for 15 min and decreased to ~ 7.9 upon CO₂ saturation. Over

this pH range, $|j_{\text{H}_2}|$ remained steady in the range of 5.2–6 mA/mg_{Ag-NP} (Figures 6A and S31). The higher $|j_{\text{H}_2}|$ in amine-free 2 M KHCO₃ compared to 2 M KCl suggests that HCO₃⁻ is a more favorable proton donor than H₂O at these pH values on Ag. Such finding agrees with the work of Marcandalli et al.⁴² on Au in CO₂-saturated KHCO₃ solutions.

Beyond HCO₃⁻ and H₂O, further comparison of $|j_{\text{H}_2}|$ in 2 M KCl + 2 M amine solutions indicates the amine-dependence of HER. As shown in Figure 6A, some amines, such as DMAE and BAPN, exhibit much higher $|j_{\text{H}_2}|$ than that observed for amine-free 2 M KHCO₃, whereas others like MEA and AMP are similar to that of 2 M KHCO₃. Such an observation can be rationalized if ammonium cations like DMAEH⁺ and BAPNH⁺ are more favorable proton donors than HCO₃⁻ for HER. This result is significant as it shows that amines present in reactive capture solutions can indeed participate directly in electrochemical reactions and affect the CO FE. On the other hand, other ammonium cations like MEAH⁺ and AMPH⁺ may be comparable or even worse proton donors for HER than HCO₃⁻, leading to similar $|j_{\text{H}_2}|$. Notably, the presence of HCO₃⁻ due to the hydrolysis of carbamate (K_c in Figure 2B) seems to impose a lower bound on $|j_{\text{H}_2}|$ in 2 M KCl + 2 M amine solutions, which may hinder the ability to suppress HER past a certain point by tailoring the amine structure. Fully understanding the relationship between the chemical structure of ammonium cations and their resulting efficacy as proton donors and/or interactions with intermediates of HER is of considerable interest to suppress HER and enhance CO FE, but such investigations are beyond the scope of this work.

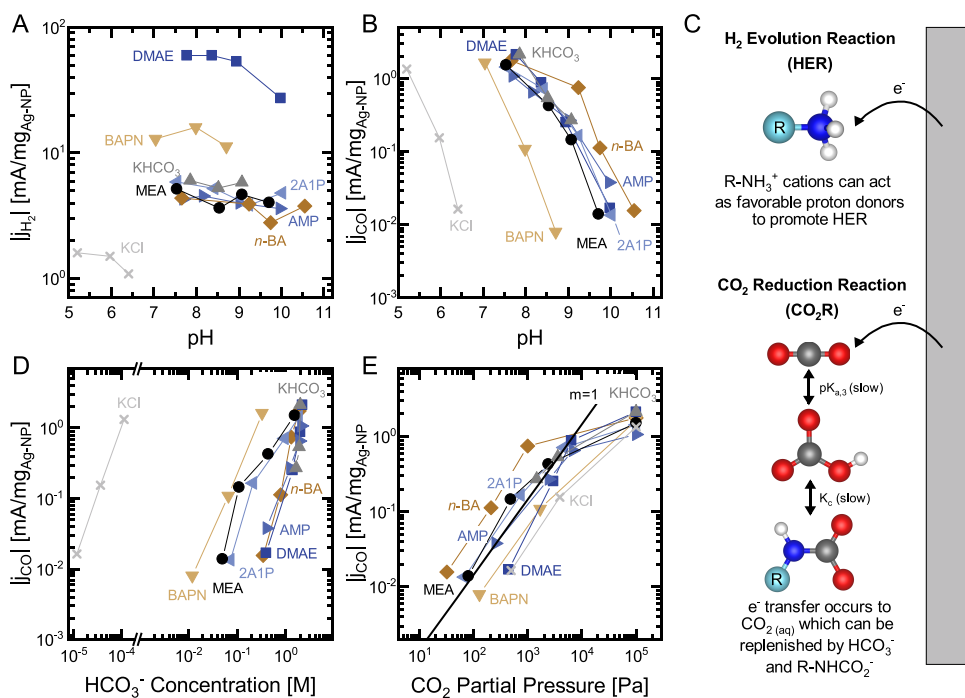


Figure 6. (A) Absolute value of H₂ partial current density (j_{H_2}) vs pH for 2 M KCl + 2 M amine solutions [MEA (circle), BAPN (inverted triangle), n-BA (diamond), 2A1P (left-pointing triangle), AMP (right-pointing triangle), and DMAE (square)] as well as amine-free 2 M KHCO₃ (triangle) and 2 M KCl (cross). Partial current is based on the current density at $-1.30\text{ V}_{\text{SHE}-\text{IR}}$ and the FE of H₂ production from GC measurements. (B) Absolute value of CO partial current density (j_{CO}) vs pH. (C) Schematic showing the proposed influence of amines on the hydrogen evolution reaction (HER) and CO₂ reduction (CO₂R). Some ammonium cations were found to be more favorable proton donors for HER than H₂O and HCO₃⁻, leading to enhanced HER activity. Electron transfer during CO₂R is proposed to occur to dissolved CO₂ in the electrolyte, which can be replenished by HCO₃⁻ and carbamate (R-NHCO₂⁻), though this process can be slow relative to CO₂R. (D) CO partial current density (j_{CO}) vs HCO₃⁻ concentration. HCO₃⁻ concentration of amine-free 2 M KHCO₃ and 2 M KCl is estimated using the VLE model (Figure S32). (E) CO partial current density (j_{CO}) vs CO₂ partial pressure. Details from NMR quantification, product quantification, and electrochemical experiments can be found in the Supporting Information.

Beyond HER, proton donors also participate directly in CO₂R, further motivating the study of the proton-donating nature of ammonium cations. We next consider the partial current density of CO production, j_{CO} , for 2 M KCl + 2 M amine solutions as well as amine-free 2 M KHCO₃ and 2 M KCl to understand the role of amines directly on CO₂R activity.

CO₂R Proceeds via e⁻ Transfer to CO₂ in Amine Capture Solutions. The partial current density for CO production, j_{CO} , shows only a weak amine-dependence, further suggesting that amines do not directly participate in CO₂R. Figure 6B shows that all of the considered amines follow a very similar overall trend, starting at low j_{CO} ~0.01 mA/mg_{Ag-NP} at higher pH values and increasing to a maximum ~1–2 mA/mg_{Ag-NP} under CO₂-saturated conditions. For instance, MEA has a j_{CO} of only 0.01 mA/mg_{Ag-NP} at pH 9.7, which increased to 1.4 mA/mg_{Ag-NP} at pH 7.6. Interestingly, with decreased or increased amine pK_a , this trend is shifted either to lower (BAPN) or to higher (n-BA) pH values, respectively (Figure 6B). Significantly, the relationship between j_{CO} and pH for 2 M KHCO₃ shows a very similar trend to amine-containing solutions (though over a narrower pH range), starting at 0.27 mA/mg_{Ag-NP} for pH 9.1 and increasing to 2.1 mA/mg_{Ag-NP} at pH 7.9. The value of j_{CO} in 2 M KCl also increased significantly with decreasing pH, from 0.02 mA/mg_{Ag-NP} at pH 6.4 to 1.3 mA/mg_{Ag-NP} at pH 5.2.

Given the weak amine-dependence of j_{CO} and the absence of a correlation with carbamate concentration (Figure S33), we

next considered possible correlations of j_{CO} with the HCO₃⁻ concentration and CO₂ partial pressure to determine whether CO₂R primarily occurs via electron transfer to HCO₃⁻ or dissolved CO₂ in amine-based capture solutions. Plotting the j_{CO} of 2 M KCl + 2 M amine solutions against either the concentration of HCO₃⁻ (Figure 6D) or the CO₂ partial pressure (Figure 6E) results in a positive correlation. However, it is important to recall that increasing CO₂ partial pressure in amine solutions leads to decreased pH (Figure 1) and that decreased pH increases the hydrolysis of carbamate to bicarbonate (Figure 2). Therefore, the CO₂ partial pressure and concentration of HCO₃⁻ in amine-containing solutions are strongly correlated (Figure S34). While the CO₂ partial pressure and concentration of HCO₃⁻ in amine-free 2 M KCl and 2 M KHCO₃ are also correlated despite lacking the carbamate hydrolysis pathway (Figure S35), the amount of HCO₃⁻ in 2 M KCl is ~4 orders of magnitude smaller (<0.1 mM) than in 2 M KHCO₃, which should lead to reduced j_{CO} if HCO₃⁻ is the active species for CO₂R. Instead, plotting j_{CO} vs [HCO₃⁻] (Figure 6D) shows that 2 M KCl has very similar j_{CO} as in 2 M KHCO₃, indicating that [HCO₃⁻] alone is an insufficient descriptor of j_{CO} .

On the other hand, when plotting j_{CO} against CO₂ partial pressure in Figure 6E, all electrolytes—including those with and without amines—collapse onto a single line with scatter < ~1.3 orders of magnitude. Plotting j_{CO} against the concentration of dissolved CO₂ from the VLE model also resulted in a single line for all electrolyte compositions (Figure

S36). Such correlation with the concentration of dissolved CO_2 is expected as the CO_2 partial pressure is related to the concentration of dissolved CO_2 via Henry's law,⁴³ allowing CO_2 partial pressure to serve as a readily accessible measure of the concentration of dissolved CO_2 in our experiments. Such an apparently universal correlation between $|j_{\text{CO}}|$ and CO_2 partial pressure/dissolved CO_2 concentration strongly suggests that CO_2R occurs via electron transfer to dissolved CO_2 in the electrolyte in all cases. Such a finding is further supported by a slope of $m = 1$ in Figure 6E, consistent with a first-order dependence of $|j_{\text{CO}}|$ on the CO_2 partial pressure, as was also observed by Wuttig et al.¹⁹ and Dunwell et al.²⁰ in amine-free NaHCO_3 solutions. Moreover, very recently, Shen et al.²³ have also observed a linear correlation between j_{CO} and CO_2 partial pressure in MEA-containing electrolytes by studying CO_2R on Ag in the transport-limited regime. Interestingly, Wuttig et al.¹⁹ further observed a zeroth-order dependence of $|j_{\text{CO}}|$ on the concentration of HCO_3^- (from added NaHCO_3), which was not observed in our study due to the correlation between CO_2 partial pressure and HCO_3^- concentration (Figure S34). However, the absence of correlation between $|j_{\text{CO}}|$ and HCO_3^- concentration can be confirmed by noting $|j_{\text{CO}}|$ in CO_2 -saturated, amine-free 2 M KCl ($1.3 \text{ mA/mg}_{\text{Ag-NP}}$) is very similar to that in CO_2 -saturated MEA electrolytes ($1.5 \text{ mA/mg}_{\text{Ag-NP}}$), despite having ~ 4 orders of magnitude less bicarbonate (Figure 6D).

Increasing CO FE requires decreasing HER activity in amine-based capture solutions. Plotting the partial current for CO production $|j_{\text{CO}}|$ against the partial current for H_2 production $|j_{\text{H}_2}|$ in Figure 7A reveals mostly vertical lines for each electrolyte composition, where with decreasing pH due to increasing CO_2 partial pressure, $|j_{\text{CO}}|$ increases, while $|j_{\text{H}_2}|$ remains \sim constant. By overlaying theoretical lines of fixed CO FE given by $j_{\text{CO}} = \text{FE}_{\text{CO}}/(1 - \text{FE}_{\text{CO}}) \times j_{\text{H}_2}$, we see that increasing CO FE in different electrolyte compositions is largely governed by decreasing $|j_{\text{H}_2}|$ (Figures 7A,B and S37). For instance, CO_2 -saturated DMAE has a low CO FE of $\sim 3.5\%$ due to its high $|j_{\text{H}_2}| = 60 \text{ mA/mg}_{\text{Ag-NP}}$, while CO_2 -saturated MEA has a much higher CO FE of $\sim 19\%$ due to its lower $|j_{\text{H}_2}| = 5.1 \text{ mA/mg}_{\text{Ag-NP}}$. Hence, from Figure 7, it is also possible to rationalize why amine-free 2 M KCl had the highest observed CO FE, which stems from the absence of favorable protons donors for HER like HCO_3^- and ammonium cations.

Replenishing Dissolved CO_2 with Bicarbonate or Carbamate Is Slow. Notably, the small scatter of ~ 1.3 orders of magnitude observed in the correlation between $|j_{\text{CO}}|$ and CO_2 partial pressure among amine-containing solutions in Figure 6E does not arise from experimental error but instead appears to be related to intrinsically different CO_2R kinetics in solutions with different amines (Figure S38). To further understand the origin, we further probed whether $|j_{\text{CO}}|$ and $|j_{\text{H}_2}|$ in our experiments were limited by the reaction kinetics, mass transport, or both. Both partial current densities showed an approximately linear relationship between $\log(|j|)$ and the applied potential (from $-1.20 \text{ V}_{\text{SHE-iR}}$ to $-1.40 \text{ V}_{\text{SHE-iR}}$) in CO_2 -saturated 2 M KCl + 2 M 2A1P (Figure S39). Given that decreasing the potential below $-1.30 \text{ V}_{\text{SHE-iR}}$ led to an exponential increase in partial current density, we can conclude that the potential of $-1.30 \text{ V}_{\text{SHE-iR}}$ used above is not in the high overpotential regime that is dominated by mass transport only. However, both partial current densities at fixed overpotential also increased with increasing rate of stirring in

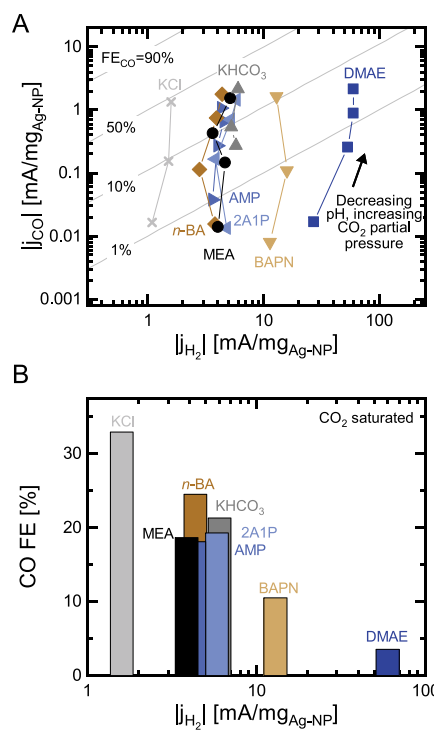


Figure 7. (A) Absolute value of CO partial current density ($|j_{\text{CO}}|$) vs H_2 partial current density ($|j_{\text{H}_2}|$) for 2 M KCl + 2 M amine solutions [MEA (circle), BAPN (inverted triangle), *n*-BA (diamond), 2A1P (left-pointing triangle), AMP (right-pointing triangle), and DMAE (square)] as well as amine-free 2 M KHCO_3 (triangle) and 2 M KCl (cross). Partial current is calculated based on the current density at $-1.30 \text{ V}_{\text{SHE-iR}}$ and the FE of H_2 or CO production from GC measurements. Lines of theoretical CO FE are given by $j_{\text{CO}} = \text{FE}_{\text{CO}}/(1 - \text{FE}_{\text{CO}}) \times j_{\text{H}_2}$. A version of this figure where the theoretical lines are defined by $\text{FE}_{\text{CO}} + \text{FE}_{\text{H}_2} = 80\%$ (20% goes to other products) is shown in Figure S37. (B) FE of CO production vs $|j_{\text{H}_2}|$.

the catholyte compartment of the H cell (Figure S40), indicating that $-1.30 \text{ V}_{\text{SHE-iR}}$ is not in the low overpotential regime that is dictated only by electrochemical reaction kinetics either. Therefore, both $|j_{\text{CO}}|$ and $|j_{\text{H}_2}|$ acquired above are in the moderate overpotential regime which is governed by both electrochemical reaction kinetics and mass transport.

In a mixed kinetics-transport regime, the kinetically limited current density is well-approximated by the Tafel relationship⁴⁴ as $j \approx C_1[\text{CO}_2, \text{aq}] \exp(C_2\eta)$ (where C_1 and C_2 are constants and η is the applied overpotential), which gives rise to a linear relationship between the current density j and $[\text{CO}_2, \text{aq}]$. Similarly, the mass transport limited current density,⁴⁵ when there is no replacement of CO_2, aq by HCO_3^- , is given by $j_{\text{lim}} \approx C_3[\text{CO}_2, \text{aq}]$ (where C_3 is a constant) and also gives rise to a linear relationship. Both of these are consistent with the first-order dependence of $|j_{\text{CO}}|$ on the CO_2 partial pressure observed in Figure 6E. However, Dunwell et al.²⁰ used ¹³C isotopic labeling to show that dissolved ¹³ CO_2 could be replenished by $\text{H}^{12}\text{CO}_3^-$ in the electrolyte. If this process were very fast in our system, then the mass transport limited current density for CO_2R would also be first-order in $[\text{HCO}_3^-]$, which is not observed in Figure 6D. Moreover, the estimated replenishment rate of CO_2, aq by HCO_3^- , determined using $[\text{HCO}_3^-]$ from the VLE model along with the published reaction rate constant (see Supporting Information for details),⁴⁶ was $< 0.08 \text{ mA/mg}_{\text{Ag-NP}}$, which is much lower than the observed $|j_{\text{CO}}| > 1 \text{ mA/mg}_{\text{Ag-NP}}$.

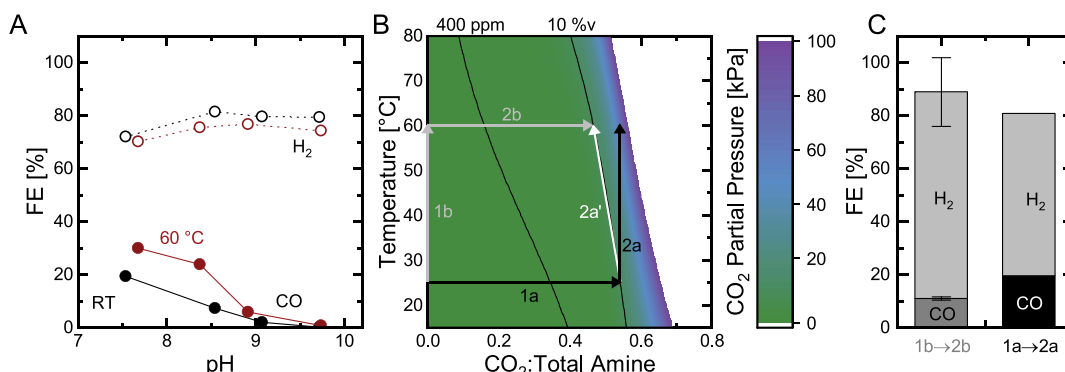


Figure 8. (A) FE of CO (filled symbols) and H₂ (open symbols) production vs pH from potentiostatic measurements at $-1.30\text{ V}_{\text{SHE}-\text{IR}}$ for 2 M KCl + 2 M MEA at room temperature (black circle) and at 60 °C (red circle). (B) Phase diagram of the equilibrium CO₂ partial pressure vs CO₂ loading and temperature from the VLE model. Arrows indicate different processes, where 1a and 2b are the isothermal sparging of 10 v% CO₂, 1b and 2a are heating of the closed system (mass is conserved), and 2a' is heating of the open system at constant CO₂ partial pressure. (C) FE of CO and H₂ production of 2 M KCl + 2 M MEA at 60 °C and $-1.30\text{ V}_{\text{SHE}-\text{IR}}$ based on the method of solution preparation, where 1b → 2b was first heated to 60 °C and then sparged with 10 v% CO₂, while 1a → 2a was first sparged with 10 v% CO₂ at room temperature and then heated to 60 °C as a closed system. Details of the VLE model, product quantification, and electrochemical experiments can be found in the Supporting Information. Error bars for 1b → 2b are from two independent measurements.

mg_{Ag-NP}. We therefore conclude that the replacement of dissolved CO₂ by bicarbonate is too sluggish to lead to significantly increased $|j_{\text{COL}}$ (e.g., $\gg 1$ order of magnitude), even with increasing [HCO₃⁻] for a given CO₂ partial pressure, in agreement with the work of Wuttig et al.¹⁹ in amine-free NaHCO₃ solutions. Nevertheless, CO₂-saturated electrolytes of similar $|j_{\text{H2I}}$ did show increasing CO FE with increasing bicarbonate concentration (Figure S41A), which suggests that the replacement of dissolved CO₂ by bicarbonate might contribute to the more modest ~ 1.3 orders of magnitude spread in $|j_{\text{COL}}$ for different amines at fixed CO₂ partial pressure. However, increasing CO FE is also observed with increasing pH of the CO₂-saturated solution (Figure S41B) or could further stem from changing kinetics due to interactions between amines and CO₂R intermediates or even non-zero contributions from the direct electroreduction of carbamate at sufficiently large overpotentials,²³ motivating further investigation into the true causality of the amine-dependence of CO₂R activity in future work.

Thermal “Upgrade” of the CO₂ Partial Pressure Increases CO FE. As a final parameter, we examined the influence of temperature on CO₂R in amine-containing solutions. Without CO₂, increasing the temperature from 25 to 60 °C results in a significant decrease in solution pH from 12.3 to 11.3. Such a decrease in pH can be attributed to decreasing MEA pK_{a,2} with increasing temperature from 9.5³⁶ at 25 °C to 8.5⁴⁷ and 60 °C. Given the strong qualitative agreement between our NMR and modeled speciation results in Figures 2, S15, S18, and S21, we here use only the modeled speciation of 2 M KCl + 2 M MEA at 25 °C and 60 °C to investigate the influence of temperature and avoid noisy signals encountered with NMR measurements at elevated temperature. As shown in Figure S42, increasing the temperature from 25 to 60 °C decreases the maximum concentration of carbamate from 0.84 to 0.77 M as well as the concentration of HCO₃⁻ at the CO₂-saturated state from 0.76 to 0.37 M. The combined effect of decreasing carbamate and HCO₃⁻ with increasing temperature decreased CO₂ loading at a CO₂ partial pressure of 1 atm, from 0.69 CO₂:total amine at 25 °C to 0.56 at 60 °C. Similar to the trend observed at room temperature (RT), the CO FE increases with decreasing pH at 60 °C, from

<1% at pH 9.9 to 30% at the CO₂-saturated pH of 7.7 (Figures 8A and S43), but the CO FE at 60 °C was modestly higher than that at RT.

We finally considered how CO FE is impacted when the temperature under which the solution captures CO₂ differs from the temperature at which electrochemistry is performed. Figure 8B shows a phase diagram based on the modeled speciation of 2 M KCl + 2 M MEA, which gives the CO₂ partial pressure as a function of the CO₂ loading (horizontal axis) and temperature (vertical axis). Moving horizontally corresponds to changing the CO₂ partial pressure to which the capture solution is exposed and allowing it to reach equilibrium. For instance, Process 1a in Figure 8B corresponds to sparging a capture solution with 10 v% CO₂ gas at ambient pressure and 25 °C. We here highlight two distinct processes by which to move to higher temperature (denoted as 2a and 2a') subsequent to Process 1a. Process 2a corresponds to heating a closed system, where mass is conserved such that the CO₂ loading remains constant, but partial pressure increases beyond 10 v%. In contrast, Process 2a' corresponds to heating an open system that remains in equilibrium with a gas stream of 10 v% CO₂ partial pressure. Since higher CO₂ partial pressure increases CO FE and $|j_{\text{COL}}$ as discussed above, increasing the temperature of the CO₂-loaded solution in the manner of Process 2a can be used to “upgrade” the CO₂ partial pressure and enhance CO₂R.

To test this hypothesis, we compared the CO FE of 2 M KCl + 2 M MEA saturated under 10 v% CO₂, where the electrochemistry was conducted at 60 °C, but the order of sparging and heating was altered. In the 1b → 2b case, we first heated the CO₂-free solution to 60 °C, following which the solution was brought to equilibrium while sparging 10 v% CO₂, leading the pH to stabilize at 8.4 (Figure S44). On the other hand, in the 1a → 2a case, we first equilibrated the solution with 10 v% CO₂ at RT, which reached a pH of 8.3. Following this, the cell was sealed and heated it to 60 °C, during which the pH further decreased to 7.7 (Figure S44), consistent with Process 2a leading to an increase in CO₂ partial pressure. Significantly, leveraging this thermal “upgrading” process led to significantly increased CO FE, from 11% for the 1b → 2b case to 20% for the 1a → 2a case (Figure 8C). Critically, such

heating of the CO₂-loaded solution provides a pathway to increase the CO₂ partial pressure during electrochemistry independently of the capture environment.

DISCUSSION

The significant influence of pH and CO₂ partial pressure on the CO FE in amine-containing solutions has critical implications for future studies on integrated capture and conversion. For instance, results obtained from solutions equilibrated under pure CO₂^{12,22} with ~0.69 CO₂/amine give unrealistically high CO FE compared to those expected under realistic reactive capture conditions from flue gas (with 12–14 v% CO₂¹⁰ and ~0.56 CO₂/amine) or from direct air capture (with ~400 ppm CO₂³³ and ~0.31 CO₂/amine). Most rigorously, capture solutions to be used in subsequent electrochemical conversion should be generated in the laboratory under conditions representative of the target application. This can, however, be impractical given the long time (>40 h) required to equilibrate capture solutions from dilute CO₂ sources (Figure 1A). We therefore recommend defining the solution state (e.g., pH) in an experiment under the conditions of the target application (such as flue gas or direct air capture) but then recreating that solution state in subsequent experiments through sparging pure CO₂ and N₂ with active pH monitoring (Figure S45). As research into reactive capture progresses, we further anticipate that considering contaminants from the capture environment such as O₂ from direct air capture as well as SOx and NOx from flue gas will be critical, but this will add further complexity.

Another consideration on integrating CO₂ capture and conversion is the crossover of dissolved inorganic carbon (DIC) to the anode⁴⁸ (i.e., the “carbonate problem”⁴⁹). Anionic DIC species like (bi)carbonate can migrate through anion exchange membranes (AEMs), significantly reducing carbon efficiency by as much as ~70%.⁵⁰ The presence of amines changes the identities and concentrations of anionic DIC species, which may alter the crossover of DIC.⁵ As discussed above, the concentrations of anionic DIC species like (bi)carbonate and carbamate depend significantly on the CO₂ partial pressure of the capture stream, where at low CO₂ partial pressure, the dominant species is carbamate. The ability to develop an AEM that excludes carbamate has, to the best of our knowledge, not been considered in the literature but might be realistic given the bulky nature of the carbamate anion or by altering the amine structure. On the other hand, even with 800 ppm CO₂, the combined (bi)carbonate concentration is 0.13 M for 2 M KCl + 2 M MEA (Figure 1F). While such (bi)carbonate concentration may be smaller compared to some conventional CO₂R electrolytes, it is by no means negligible, indicating that the crossover of (bi)carbonate remains a key challenge to overcome for electrochemical reactive capture systems. While the combined (bi)carbonate concentration can be further decreased by leveraging primary amines of decreasing pK_a, it cannot be eliminated altogether. Moreover, primary amines of decreasing pK_a can decrease CO₂ uptake kinetics and loading, likely adding cost to the absorber.

Additional design approaches, such as the use of cation exchange membranes (CEMs) or bipolar membranes (BPMs), may therefore still be prudent for the integrated capture and conversion of CO₂, though each come with their own associated challenges. For instance, K⁺ or similar metal cations are the dominant charge carriers in CEMs under neutral or basic conditions, where these metal cations fail to neutralize

the generated OH⁻ in the catholyte, driving a pH imbalance over time that can further lead to salt precipitation.⁵¹ Moreover, we observed that amine species can crossover the CEM (Figure S46), which warrants further study if CEM systems are pursued for integrated capture/conversion. Finally, the longevity and overpotentials imposed by BPM remain as significant challenges.⁵²

From amine-free 2 M KCl having the highest CO FE in Figure 7B, one might reasonably conclude that the presence of amines to capture CO₂ and form carbamate and bicarbonate is detrimental as this introduces more facile proton donors for HER like ammonium cations and bicarbonate, which decreases CO FE relative to amine-free 2 M KCl. However, DIC like bicarbonate and carbamate can potentially replenish dissolved CO₂ in the electrolyte,^{19,20} circumventing the first-order dependence of $|j_{CO}|$ on CO₂ partial pressure (Figure 6E) when the mass transport of dissolved CO₂ is limiting. Unfortunately, above, we saw that the replenishment of dissolved CO₂ is slow, which motivates a pursuit of future strategies to catalyze the dehydration of bicarbonate, as well as the hydrolysis of carbamate. In the case that DIC can readily replenish dissolved CO₂, amines offer an advantage as they can have high DIC concentrations—even higher than the solubility limit of KHCO₃ (2.9 M at 20 °C⁵³). To demonstrate this, we prepared an amine solution with ~4.5 M MEA, which reached a DIC concentration of ~3.2 M (Figure S47) and a maximum CO FE of 33% (Figure S48), equivalent to amine-free 2 M KCl (the highest CO FE in this study). However, excessively high amine concentrations can lead to significant increases in electrolyte viscosity.⁵⁴ Also notable in Figure 7A is that some amine-containing solutions like MEA showed comparable $|j_{H2}|$ and $|j_{CO}|$ to amine-free 2 M KHCO₃, indicating that the inclusion of well-selected amines does not negatively influence the selectivity or kinetics of CO₂R. Such a finding is highly encouraging as even though the inclusion of CO₂ sorbents like amines into the electrolyte increases complexity in reactive capture systems, it does not necessarily impede the subsequent electrochemical reduction of CO₂.

Unlocking the ability of DIC in the form of bicarbonate and carbamate to readily replenish CO₂ at the electrode surface necessitates further study of the kinetics of bicarbonate dehydration and carbamate hydrolysis, as well as enhanced understanding of the out-of-equilibrium solution chemistry near the electrode surface. In this work, we considered the bulk solution pH which, along with the applied current density, defines the boundary conditions of the interface. Recent work in amine-free bicarbonate electrolytes on Au electrodes⁵⁵ has shown that the interfacial pH can be >11 even at relatively modest current densities <3 mA/cm². Given that HER kinetics become more facile with increasing pH,⁴¹ such increased interfacial pH can lead to decreased CO FE.⁵⁵ It is therefore essential to not just enhance the availability of CO₂ at the electrode surface but also efficiently remove the formed OH⁻, such as through transport or neutralization. The inclusion of amines introduces further complexity into the interfacial solution chemistry,¹⁰ which provides both challenges and opportunities to increase the efficiency of CO₂R.

CONCLUSIONS

In this work, systematic studies of CO₂R to CO on Ag catalysts were performed to assess the role of amines on the CO₂R from reactive capture solutions. We first showed that pH of the CO₂-loaded solution varied significantly with the CO₂ partial

pressure of the capture stream. We further used ^1H and ^{13}C NMR, along with a VLE model to quantify the speciation of amine capture solutions, uncovering a significant pH-dependence. During CO_2R , the CO FE was found to increase greatly with decreasing solution pH, ultimately correlating most strongly with the CO_2 partial pressure. Through studying amines of different $\text{p}K_a$ and with different propensities to form carbamate, we found that the intrinsic CO_2R kinetics showed a weak amine-dependence, but HER kinetics could be significantly enhanced by some ammonium cations that were favorable proton donors, whereas other ammonium cations were comparable or worse proton donors than bicarbonate. We further found that the CO partial current density showed a first-order dependence on CO_2 partial pressure, consistent with CO_2R occurring via electron transfer to dissolved CO_2 as the major electrochemically active species in amine-containing solutions, rather than carbamate (at least with the all-Ag electrodes used in this study). As a result, amines in reactive capture solutions can serve as a reservoir of dissolved inorganic carbon that can serve to replenish dissolved CO_2 in the electrolyte, alleviating mass transfer and transport limitations without directly participating in the reaction. Finally, we demonstrated an approach to “thermally upgrade” the CO_2 partial pressure by heating the CO_2 -loaded solution in a closed system which led to increased CO FE. This work highlights the need to precisely define and recreate the CO_2 partial pressure of the target application for future studies to generate representative performance in a laboratory setting.

ASSOCIATED CONTENT

Supporting Information

The Supporting Information is available free of charge at <https://pubs.acs.org/doi/10.1021/acscatal.3c02500>.

Experimental methods; NMR spectra; detailed electrochemical data; electrolyte speciation from NMR and VLE model; supplemental discussion; details of NMR quantification; details of the amine speciation VLE model; and supplemental analysis and derivations ([PDF](#))

AUTHOR INFORMATION

Corresponding Author

Betar M. Gallant — Department of Mechanical Engineering, Massachusetts Institute of Technology, Cambridge, Massachusetts 02139, United States;  orcid.org/0000-0002-4586-2769; Email: bgallant@mit.edu

Authors

Graham Leverick — Department of Mechanical Engineering, Massachusetts Institute of Technology, Cambridge, Massachusetts 02139, United States;  orcid.org/0000-0001-8541-4381

Elizabeth M. Bernhardt — Department of Mechanical Engineering, Massachusetts Institute of Technology, Cambridge, Massachusetts 02139, United States

Aisyah Ilyani Ismail — Research Centre for Carbon Dioxide Capture and Utilisation (CCDCU), School of Engineering and Technology, Sunway University, 47500 Petaling Jaya, Malaysia

Jun Hui Law — Research Centre for Carbon Dioxide Capture and Utilisation (CCDCU), School of Engineering and

Technology, Sunway University, 47500 Petaling Jaya, Malaysia

A. Arifutzzaman — Research Centre for Carbon Dioxide Capture and Utilisation (CCDCU), School of Engineering and Technology, Sunway University, 47500 Petaling Jaya, Malaysia

Mohamed Kheireddine Aroua — Research Centre for Carbon Dioxide Capture and Utilisation (CCDCU), School of Engineering and Technology, Sunway University, 47500 Petaling Jaya, Malaysia; Sunway Materials Smart Science & Engineering Research Cluster (SMS2E), Sunway University, Petaling Jaya, Selangor 47500, Malaysia; School of Engineering, Lancaster University, Lancaster LA1 4YW, U.K.;  orcid.org/0000-0002-9388-5439

Complete contact information is available at: <https://pubs.acs.org/10.1021/acscatal.3c02500>

Notes

The authors declare no competing financial interest.

ACKNOWLEDGMENTS

The authors gratefully acknowledge financial support provided by Sunway University, Malaysia through project No. RCO-FOR-MIT-001-2020. This work made use of the MRSEC Shared Experimental Facilities at MIT, supported by the National Science Foundation under Grant DMR-14-19807. E.M.B. gratefully acknowledges support from a National Science Foundation Graduate Research Fellowship under Grant No. 2141064. The authors would like to thank Dr. Bruce Adams from DCIF at MIT for his assistance in developing NMR procedures in this work. They additionally thank Dr. Sung Eun Jerng for assistance collecting SEM images.

REFERENCES

- (1) Bushuyev, O. S.; De Luna, P.; Dinh, C. T.; Tao, L.; Saur, G.; van de Lagemaat, J.; Kelley, S. O.; Sargent, E. H. What Should We Make with CO_2 and How Can We Make It? *Joule* **2018**, *2*, 825–832.
- (2) Jouny, M.; Hutchings, G. S.; Jiao, F. Carbon Monoxide Electroreduction as an Emerging Platform for Carbon Utilization. *Nat. Catal.* **2019**, *2*, 1062–1070.
- (3) Bui, M.; Adjiman, C. S.; Bardow, A.; Anthony, E. J.; Boston, A.; Brown, S.; Fennell, P. S.; Fuss, S.; Galindo, A.; Hackett, L. A.; Hallett, J. P.; Herzog, H. J.; Jackson, G.; Kemper, J.; Krevor, S.; Maitland, G. C.; Matuszewski, M.; Metcalfe, I. S.; Petit, C.; Puxty, G.; Reimer, J.; Reiner, D. M.; Rubin, E. S.; Scott, S. A.; Shah, N.; Smit, B.; Trusler, J. P. M.; Webley, P.; Wilcox, J.; Mac Dowell, N. Carbon Capture and Storage (CCS): The Way Forward. *Energy Environ. Sci.* **2018**, *11*, 1062–1176.
- (4) Renfrew, S. E.; Starr, D. E.; Strasser, P. Electrochemical Approaches toward CO_2 Capture and Concentration. *ACS Catal.* **2020**, *10*, 13058–13074.
- (5) Li, M.; Irtem, E.; Iglesias van Montfort, H.-P.; Abdinejad, M.; Burdyny, T. Energy Comparison of Sequential and Integrated CO_2 Capture and Electrochemical Conversion. *Nat. Commun.* **2022**, *13*, 5398.
- (6) Rochelle, G. T. Amine Scrubbing for CO_2 Capture. *Science* **2009**, *325*, 1652–1654.
- (7) Heldebrant, D. J.; Kothandaraman, J.; Dowell, N. M.; Brickett, L. Next Steps for Solvent-Based CO_2 Capture; Integration of Capture, Conversion, and Mineralisation. *Chem. Sci.* **2022**, *13*, 6445–6456.
- (8) Siegel, R. E.; Pattanayak, S.; Berben, L. A. Reactive Capture of CO_2 : Opportunities and Challenges. *ACS Catal.* **2023**, *13*, 766–784.
- (9) Zhang, S.; Chen, C.; Li, K.; Yu, H.; Li, F. Materials and System Design for Direct Electrochemical CO_2 Conversion in Capture Media. *J. Mater. Chem. A* **2021**, *9*, 18785–18792.

- (10) Jerng, S. E.; Gallant, B. M. Electrochemical Reduction of CO₂ in the Captured State Using Aqueous or Nonaqueous Amines. *iScience* **2022**, *25*, No. 104558.
- (11) Lee, G.; Li, Y. C.; Kim, J.-Y.; Peng, T.; Nam, D.-H.; Sedighian Rasouli, A.; Li, F.; Luo, M.; Ip, A. H.; Joo, Y.-C.; Sargent, E. H. Electrochemical Upgrade of CO₂ from Amine Capture Solution. *Nat. Energy* **2021**, *6*, 46–53.
- (12) Kim, J. H.; Jang, H.; Bak, G.; Choi, W.; Yun, H.; Lee, E.; Kim, D.; Kim, J.; Lee, S. Y.; Hwang, Y. J. The Insensitive Cation Effect on a Single Atom Ni Catalyst Allows Selective Electrochemical Conversion of Captured CO₂ in Universal Media. *Energy Environ. Sci.* **2022**, *15*, 4301–4312.
- (13) Abdinejad, M.; Mirza, Z.; Zhang, X.; Kraatz, H.-B. Enhanced Electrocatalytic Activity of Primary Amines for CO₂ Reduction Using Copper Electrodes in Aqueous Solution. *ACS Sustainable Chem. Eng.* **2020**, *8*, 1715–1720.
- (14) Liu, X.; Xiao, J.; Peng, H.; Hong, X.; Chan, K.; Nørskov, J. K. Understanding Trends in Electrochemical Carbon Dioxide Reduction Rates. *Nat. Commun.* **2017**, *8*, 15438.
- (15) Back, S.; Yeom, M. S.; Jung, Y. Active Sites of Au and Ag Nanoparticle Catalysts for CO₂ Electroreduction to CO. *ACS Catal.* **2015**, *5*, 5089–5096.
- (16) Zhao, S.; Jin, R.; Jin, R. Opportunities and Challenges in CO₂ Reduction by Gold- and Silver-Based Electrocatalysts: From Bulk Metals to Nanoparticles and Atomically Precise Nanoclusters. *ACS Energy Lett.* **2018**, *3*, 452–462.
- (17) Ringe, S.; Morales-Guio, C. G.; Chen, L. D.; Fields, M.; Jaramillo, T. F.; Hahn, C.; Chan, K. Double Layer Charging Driven Carbon Dioxide Adsorption Limits the Rate of Electrochemical Carbon Dioxide Reduction on Gold. *Nat. Commun.* **2020**, *11*, 33.
- (18) Verma, S.; Hamasaki, Y.; Kim, C.; Huang, W.; Lu, S.; Jhong, H.-R. M.; Gewirth, A. A.; Fujigaya, T.; Nakashima, N.; Kenis, P. J. A. Insights into the Low Overpotential Electroreduction of CO₂ to CO on a Supported Gold Catalyst in an Alkaline Flow Electrolyzer. *ACS Energy Lett.* **2018**, *3*, 193–198.
- (19) Wuttig, A.; Yaguchi, M.; Motabayashi, K.; Osawa, M.; Surendranath, Y. Inhibited Proton Transfer Enhances Au-Catalyzed CO₂-to-Fuels Selectivity. *Proc. Natl. Acad. Sci. U. S. A.* **2016**, *113*, E4585–E4593.
- (20) Dunwell, M.; Lu, Q.; Heyes, J. M.; Rosen, J.; Chen, J. G.; Yan, Y.; Jiao, F.; Xu, B. The Central Role of Bicarbonate in the Electrochemical Reduction of Carbon Dioxide on Gold. *J. Am. Chem. Soc.* **2017**, *139*, 3774–3783.
- (21) Kim, I.; Hoff, K. A.; Mejdell, T. Heat of Absorption of CO₂ with Aqueous Solutions of MEA: New Experimental Data. *Energy Procedia* **2014**, *63*, 1446–1455.
- (22) Chen, L.; Li, F.; Zhang, Y.; Bentley, C. L.; Horne, M.; Bond, A. M.; Zhang, J. Electrochemical Reduction of Carbon Dioxide in a Monoethanolamine Capture Medium. *ChemSusChem* **2017**, *10*, 4109–4118.
- (23) Shen, K.; Cheng, D.; Reyes-Lopez, E.; Jang, J.; Sautet, P.; Morales-Guio, C. G. On the Origin of Carbon Sources in the Electrochemical Upgrade of CO₂ from Carbon Capture Solutions. *Joule* **2023**, *7*, 1260–1276.
- (24) Ringe, S.; Clark, E. L.; Resasco, J.; Walton, A.; Seger, B.; Bell, A. T.; Chan, K. Understanding Cation Effects in Electrochemical CO₂ Reduction. *Energy Environ. Sci.* **2019**, *12*, 3001–3014.
- (25) Monteiro, M. C. O.; Dattila, F.; López, N.; Koper, M. T. M. The Role of Cation Acidity on the Competition between Hydrogen Evolution and CO₂ Reduction on Gold Electrodes. *J. Am. Chem. Soc.* **2022**, *144*, 1589–1602.
- (26) Khurram, A.; Yan, L.; Yin, Y.; Zhao, L.; Gallant, B. M. Promoting Amine-Activated Electrochemical CO₂ Conversion with Alkali Salts. *J. Phys. Chem. C* **2019**, *123*, 18222–18231.
- (27) Khurram, A.; He, M.; Gallant, B. M. Tailoring the Discharge Reaction in Li-CO₂ Batteries through Incorporation of CO₂ Capture Chemistry. *Joule* **2018**, *2*, 2649–2666.
- (28) Bhattacharya, M.; Sebghati, S.; Vercella, Y. M.; Saouma, C. T. Electrochemical Reduction of Carbamates and Carbamic Acids: Implications for Combined Carbon Capture and Electrochemical CO₂ Recycling. *J. Electrochem. Soc.* **2020**, *167*, No. 086507.
- (29) Pérez-Gallent, E.; Vankani, C.; Sánchez-Martínez, C.; Anastasopol, A.; Goetheer, E. Integrating CO₂ Capture with Electrochemical Conversion Using Amine-Based Capture Solvents as Electrolytes. *Ind. Eng. Chem. Res.* **2021**, *60*, 4269–4278.
- (30) Richner, G.; Puxty, G. Assessing the Chemical Speciation during CO₂ Absorption by Aqueous Amines Using *in Situ* FTIR. *Ind. Eng. Chem. Res.* **2012**, *51*, 14317–14324.
- (31) Kortunov, P. V.; Siskin, M.; Baugh, L. S.; Calabro, D. C. *In Situ* Nuclear Magnetic Resonance Mechanistic Studies of Carbon Dioxide Reactions with Liquid Amines in Aqueous Systems: New Insights on Carbon Capture Reaction Pathways. *Energy Fuels* **2015**, *29*, 5919–5939.
- (32) Fan, G.; Wee, A. G. H.; Idem, R.; Tontiwachwuthikul, P. NMR Studies of Amine Species in MEA–CO₂–H₂O System: Modification of the Model of Vapor–Liquid Equilibrium (VLE). *Ind. Eng. Chem. Res.* **2009**, *48*, 2717–2720.
- (33) Kosaka, F.; Liu, Y.; Chen, S.-Y.; Mochizuki, T.; Takagi, H.; Urakawa, A.; Kuramoto, K. Enhanced Activity of Integrated CO₂ Capture and Reduction to CH₄ under Pressurized Conditions toward Atmospheric CO₂ Utilization. *ACS Sustainable Chem. Eng.* **2021**, *9*, 3452–3463.
- (34) Aroua, M. K.; Benamor, A.; Haji-Sulaiman, M. Z. Equilibrium Constant for Carbamate Formation from Monoethanolamine and Its Relationship with Temperature. *J. Chem. Eng. Data* **1999**, *44*, 887–891.
- (35) Conway, W.; Wang, X.; Fernandes, D.; Burns, R.; Lawrence, G.; Puxty, G.; Maeder, M. Comprehensive Kinetic and Thermodynamic Study of the Reactions of CO₂ (Aq) and HCO₃[−] with Monoethanolamine (MEA) in Aqueous Solution. *J. Phys. Chem. A* **2011**, *115*, 14340–14349.
- (36) Gupta, M.; Svendsen, H. F. Modeling Temperature Dependent and Absolute Carbamate Stability Constants of Amines for CO₂ Capture. *Int. J. Greenhouse Gas Control* **2020**, *98*, No. 103061.
- (37) England, A. H.; Duffin, A. M.; Schwartz, C. P.; Uejio, J. S.; Prendergast, D.; Saykally, R. J. On the Hydration and Hydrolysis of Carbon Dioxide. *Chem. Phys. Lett.* **2011**, *514*, 187–195.
- (38) du Preez, L. J.; Motang, N.; Callanan, L. H.; Burger, A. J. Determining the Liquid Phase Equilibrium Speciation of the CO₂–MEA–H₂O System Using a Simplified *in Situ* Fourier Transform Infrared Method. *Ind. Eng. Chem. Res.* **2019**, *58*, 469–478.
- (39) Penders-van Elk, N. J. M. C.; Fradette, S.; Versteeg, G. F. Effect of PKa on the Kinetics of Carbon Dioxide Absorption in Aqueous Alkanolamine Solutions Containing Carbonic Anhydrase at 298K. *Chem. Eng. J.* **2015**, *259*, 682–691.
- (40) CRC Handbook of Chemistry and Physics, 84th ed.; Lide, D. R., Ed.; CRC Press: Boca Raton, 2003, pp 1278.
- (41) Goyal, A.; Koper, M. T. M. The Interrelated Effect of Cations and Electrolyte PH on the Hydrogen Evolution Reaction on Gold Electrodes in Alkaline Media. *Angew. Chem., Int. Ed.* **2021**, *60*, 13452–13462.
- (42) Marcandalli, G.; Goyal, A.; Koper, M. T. M. Electrolyte Effects on the Faradaic Efficiency of CO₂ Reduction to CO on a Gold Electrode. *ACS Catal.* **2021**, *11*, 4936–4945.
- (43) Benamor, A.; Aroua, M. K. Modeling of CO₂ Solubility and Carbamate Concentration in DEA, MDEA and Their Mixtures Using the Deshmukh–Mather Model. *Fluid Phase Equilib.* **2005**, *231*, 150–162.
- (44) Bard, A. J.; Faulkner, L. R. Kinetics of Electrode Reactions. In *Electrochemical Methods: Fundamentals and Applications*, 2nd ed.; Wiley: New York, 2001, pp 87–136.
- (45) Bard, A. J.; Faulkner, L. R. Mass Transfer by Migration and Diffusion. In *Electrochemical Methods: Fundamentals and Applications*, 2nd ed.; Wiley: New York, 2001, pp 137–155.
- (46) Forster, R.; Edsall, J.; Otis, A.; Roughton, F. CO₂: Chemical, Biochemical, and Physiological Aspects. NASA SP-188; NASA, 1969, 270.

- (47) Kim, I.; Grimstvedt, A.; da Silva, E. F. Thermodynamics of Protonation of Alkanolamines in Aqueous Solutions. *Energy Procedia* **2011**, *4*, 576–582.
- (48) Ma, M.; Clark, E. L.; Therkildsen, K. T.; Dalsgaard, S.; Chorkendorff, I.; Seger, B. Insights into the Carbon Balance for CO₂ Electroreduction on Cu Using Gas Diffusion Electrode Reactor Designs. *Energy Environ. Sci.* **2020**, *13*, 977–985.
- (49) Rabinowitz, J. A.; Kanan, M. W. The Future of Low-Temperature Carbon Dioxide Electrolysis Depends on Solving One Basic Problem. *Nat. Commun.* **2020**, *11*, 5231.
- (50) O'Brien, C. P.; Miao, R. K.; Liu, S.; Xu, Y.; Lee, G.; Robb, A.; Huang, J. E.; Xie, K.; Bertens, K.; Gabardo, C. M.; Edwards, J. P.; Dinh, C.-T.; Sargent, E. H.; Sinton, D. Single Pass CO₂ Conversion Exceeding 85% in the Electrosynthesis of Multicarbon Products via Local CO₂ Regeneration. *ACS Energy Lett.* **2021**, *6*, 2952–2959.
- (51) De Mot, B.; Hereijgers, J.; Daems, N.; Breugelmans, T. Insight in the Behavior of Bipolar Membrane Equipped Carbon Dioxide Electrolyzers at Low Electrolyte Flowrates. *Chem. Eng. J.* **2022**, *428*, No. 131170.
- (52) Giesbrecht, P. K.; Freund, M. S. Recent Advances in Bipolar Membrane Design and Applications. *Chem. Mater.* **2020**, *32*, 8060–8090.
- (53) Trypuć, M.; Kielkowska, U.; Stefanowicz, D. Solubility Investigations in the KHCO₃ + NH₄HCO₃ + H₂O System. *J. Chem. Eng. Data* **2001**, *46*, 800–804.
- (54) Idris, Z.; Kummamuru, N. B.; Eimer, D. A. Viscosity Measurement of Unloaded and CO₂-Loaded Aqueous Monoethanolamine at Higher Concentrations. *J. Mol. Liq.* **2017**, *243*, 638–645.
- (55) Liu, X.; Monteiro, M. C. O.; Koper, M. T. M. Interfacial PH Measurements during CO₂ Reduction on Gold Using a Rotating Ring-Disk Electrode. *Phys. Chem. Chem. Phys.* **2023**, *25*, 2897–2906.